1249

MAY 1977 MATT-1249

CURRENT-DRIVEN INSTABILITIES AND RESULTANT ANOMALOUS EFFECTS IN ISOTHERMAL, INHOMOGENEOUS PLASMAS

BY

M. YAMADA AND H. W. HENDEL

PLASMA PHYSICS LABORATORY

PRINCETON UNIVERSITY
PRINCETON, NEW JERSEY

This work was supported by U. S. Energy Research and Development Administration Contract E(11-1)-3073. Reproduction, translation, publication, use and disposal, in whole or in part, by or for the United States Government is permitted.

DISCLAIMER

NOTICE

Printed in the United States of America.

Available from
National Technical Information Service
U. S. Department of Commerce
5285 Port Royal Road
Springfield, Virginia 22151
Price: Printed Copy $ * ; Microfiche $3.00

*Pages	NTIS Selling Price
1-50	$ 4.00
51-150	5.45
151-325	7.60
326-500	10.60
501-1000	13.60

Current-Driven Instabilities and Resultant Anomalous Effects in Isothermal, Inhomogeneous Plasmas

M. Yamada and H. W. Hendel

Princeton University, Plasma Physics Laboratory
Princeton, New Jersey 08540

MATT-1249

May 1977

CURRENT-DRIVEN INSTABILITIES AND RESULTANT ANOMALOUS EFFECTS IN ISOTHERMAL, INHOMOGENEOUS PLASMAS

by

M. Yamada and H. W. Hendel

Plasma Physics Laboratory,
Princeton University,
Princeton, New Jersey 08540

ABSTRACT

The evolution and effects of current-driven instabilities in isothermal, inhomogeneous plasmas are investigated in both theory and experiment. Successive destabilizations of four different instabilities, low-frequency drift wave, ion-cyclotron drift wave, high-frequency (continuous-spectrum ion-cyclotron) drift wave, and high-frequency electron wave, are observed in Q-device plasmas with increased current, and explained by a theory based on fluid and kinetic equations. Anomalous effects resulting from wave-particle interactions, i.e., enhanced resistivity, ion heating and electron viscosity, are compared with predictions based on quasi-linear calculations. Analogous to ion sound causing important anomalies in the transport coefficients for plasmas with $T_e/T_i \gg 1$, high-frequency, continuous-spectrum drift waves determine anomalous plasma behavior in inhomogeneous plasmas with $T_e/T_i \simeq 1$.

I. INTRODUCTION

Current-driven instabilities and turbulent heating have generally been studied in nonisothermal plasmas ($T_e >> T_i$) due to the pulsed, high voltage and high current operation used. Thus, destabilization of ion sound is expected at electron drift velocities smaller than the electron thermal velocity and should play a significant role in the interpretation: In relevant experiments ion-sound instability has usually been confirmed and theories of turbulent heating have been based on its presence. In representative work, such as that of Hamberger and Jancarik,[1] Mah et al.,[2] and Hirose et al.,[3] anomalous parallel resistivity and turbulent ion heating are observed and analyzed in terms of current-driven ion sound for $u/v_{the} < 1$ (u/v_{the} = ratio of electron drift to thermal velocity) and Buneman-Budker instability for $u/v_{the} > 1$.

Recently, however, in connection with fusion devices, interest has developed in the effects of instabilities, and in plasma heating, for $T_e/T_i \sim 1$ and $u/v_{the} < 1$. For these conditions strong ion Landau damping prevents excitation of ion sound waves. The question thus arises whether other instabilities not previously considered can be excited in isothermal plasmas and cause anomalous effects similar to those generated by ion sound in nonisothermal plasmas, especially enhanced resistivity, heating, and perpendicular thermal conductivity. This paper presents an experimental and theoretical investigation of the evolution and effects of current-driven instabilities in the isothermal, inhomogeneous plasma of the Princeton Q-1 device.

Q-device plasmas[4] are isothermal for electron rich conditions. At high plate temperatures, electron emission is much greater than ion emission, the plasma becomes negatively charged, and the sheaths adjacent to the end plates accelerate the newly surface-ionized ions into the plasma, raising the ion temperature slightly above the plate (i.e., electron) temperature. The high electron thermal conductivity connects the electrons with the infinite heat sink of the end plates, limiting electron temperature increase even in the presence of heating currents. In early current-driven work on Q-device plasmas, this limitation of the temperature ratio, $T_e/T_i \simeq 1$, and its effects (particularly the strong ion Landau damping of ion sound) were not recognized. In addition, early work was restricted in scope, concentrating only on specific measurements without (a) describing the full evolution of all current-driven instabilities, (b) identifying them, and (c) relating them to the causal electron drift velocity and the resulting anomalous effects on the plasma parameters.

Rynn reported the first studies of Q-device I-V characteristics and observed onset of oscillations (at 4, 11, and 65 kHz)[5] beyond the current maximum; he explained the instability then "tentatively as due to run-away electrons." An estimate of sheath effects by Rynn[6] and ion heating studies based on Doppler broadening in Q-device Barium-plasmas by Hinnov et al.[7] do not consider instability effects, and more recent heating studies by Watanabe and Tanaca[8] were performed

in single-ended operation and do not contain measurements of instability dispersion relations and electron drift velocities.

Buchelnikova and co-workers have studied current-driven instabilities and their effects in Q-devices in great detail. The main instability developing with increased current was at first determined to be ion sound[9] and later ion-cyclotron instability.[10] Enhanced diffusion and ion heating were observed and related to the latter instability. Collisional drift waves, excited by parallel current at electron drift velocities above the ion-sound velocity, are discussed by Ellis and Motley[11] with detailed comparisons of experimental results and dispersion relations. Our group reported briefly the successive destabilization of three different instabilities with increased current.[12]

Theoretical work by Jackson predicts ion sound to be stable for isothermal plasmas and drift velocities below the electron thermal velocity.[13] For an infinite, collisionless plasma and at electron drift velocities an order of magnitude above the ion-sound velocity (but below the electron thermal velocity), the electrostatic ion-cyclotron wave was predicted by Drummond and Rosenbluth.[14] A theory of anomalous resistivity at low electric fields based on drift-type instabilities was given by Coppi and Mazzucato[15] to explain stellarator and tokamak results. Cyclotron frequency modes were included but apparently higher-frequency, continuous-spectrum drift waves were not considered, which can give a more pronounced resistivity increase.

Recognizing some of the discrepancies described, we have attempted a comprehensive investigation of the evolution of current-driven instabilities in isothermal plasmas and of the resulting anomalous effects. With increasing current (u/v_{the} = 0 to 1/3), successive destabilization of four different instabilities is observed. Onset drift velocities and anomalous effects are in general agreement with predictions. (1) Onset of current-driven collisional ∇n drift waves ($f \simeq 3$ kHz $\simeq 10^{-3} f_{pi}$; $u \simeq 10\, v_{thi} \simeq 1/50\, v_{the}$) leads to anomalous diffusion. (2) Onset of discrete-spectrum, resonantly-driven ion-cyclotron drift waves ($f = 1.15\, f_{ci} = 1/20\, f_{pi}$; $u \simeq 1/10\, v_{the}$) produces slight anomalous resistivity and ion heating. (3) Onset of the recently identified[16] continuous-spectrum ion-cyclotron drift wave ($f \simeq 0 - 1/4\, f_{pi}$) generates strong anomalous resistivity, current inhibition, and intense ion heating.[17] (4) Onset of a fourth instability ($f = 5\text{-}100\, f_{pi}$; $u \simeq 1/3\, v_{the}$) causes relaxation of the radial electron-temperature gradient. In the presence of the latter three instabilities both electron and ion temperatures are mainly determined by wave-particle interactions. The third instability, the continuous-spectrum ion-cyclotron drift wave, is of special interest: It causes anomalous effects similar to an ion sound wave, but can exist in a plasma where ion sound is ion Landau damped. Finally, the instabilities observed are dominated by the radial inhomogeneities of the plasma column. Table 1 summarizes the characteristic features of these four instabilities.

Thus, general similarity is found between previous observations[1-3] in nonisothermal plasmas and the present work in isothermal plasmas. In both cases a succession of instabilities with continuously higher frequency, phase velocity, and growth rate is destabilized by the increased parallel electron drift velocity. Moreover, a new instability of the inhomogeneous plasma is identified which plays a role comparable to that of ion sound in homogeneous, nonisothermal plasmas. The anomalous resistivity produced is measured locally inside the plasma and cannot be due to sheath effects but is generated by wave-particle interactions.

Section II contains the theory of low- and high-frequency instabilities in inhomogeneous isothermal plasmas with electron current, focussing our attention on high-frequency drift waves with $\omega \gtrsim \omega_{ci}$. Section III describes the experimental apparatus and techniques, and Section IV the results. Parts of this work have been reported previously in abbreviated form.[16,17]

II. THEORY — INSTABILITIES IN INHOMOGENEOUS ISOTHERMAL PLASMA

We now investigate the theoretical aspects of current-driven instabilities in inhomogeneous, isothermal, fully-ionized, linear plasmas confined by a strong magnetic field, taking into account radial gradients of n_e, T_e, and T_i in the plasma column and collisional effects. We derive general dielectric constants (polarizabilities) of electrons and ions separately and from them obtain the relevant dispersion relations for the different phase velocity regimes and wave frequencies.

Consider a plasma slab with uniform magnetic field B in the z direction; all gradients are assumed in the x direction, and a drift velocity u of the electrons in the z direction. In the absence of collisions, the total kinetic energy of a particle, $\frac{1}{2}mv^2$, is a constant of motion. Since the system is translationally invariant in the y and z directions, the canonical momenta $p_y = mv_y + (qB/C)x$ and $p_z = mv_z$ should also be conserved. Unperturbed distributions should then be expressed as functions of those three conserved quantities.[18,19] The simplest choice of such a function, which would reduce to the Maxwellian in the absence of the inhomogeneities, may be given by

$$f_{\sigma 0}(x,\vec{v}) = \left(\frac{m_\sigma}{2\pi T_\sigma(x)}\right)^{3/2} n_\sigma(x) \left[-\frac{m_\sigma(\vec{v} - u_\sigma\hat{z})^2}{2T_\sigma(x)}\right] , \quad (1a)$$

where σ denotes electrons or (singly charged) ions; density and temperature of each species are expressed as

$$n_\sigma = n_0\left[1 + \alpha\left(x + \frac{v_y}{\omega_{c\sigma}}\right)\right] \quad , \tag{1b}$$

$$T_\sigma = T_{\sigma 0}\left[1 + \beta_\sigma\left(x + \frac{v_y}{\omega_{c\sigma}}\right)\right] \quad , \tag{1c}$$

and

$\omega_{c\sigma}$ = cyclotron frequency of σ species.

We assume that the spatial density variation is small over a Larmor radius, so that

$$\left|\frac{1}{n}\frac{dn_\sigma}{dx}\right| \rho_\sigma < 1 \quad . \tag{2}$$

The first order Boltzman equation may be written:

$$\frac{\partial f_{\sigma 1}}{\partial t} + \vec{v}\cdot\frac{\partial f_{\sigma 1}}{\partial \vec{v}} + \frac{q}{m}\left(\vec{E} + \frac{\vec{v}}{c} \times \vec{B}\right)\frac{\partial f_{\sigma 0}}{\partial v} = -\left(\frac{\partial f}{\partial t}\right)_{c\sigma} \quad . \tag{3}$$

The right side of Eq. (3) represents the collisional loss term of the σ species.

For wavelengths comparable or shorter than the mean-free path, we adopt the Batnagar-Gross-Krook (BGK)[20] collision term

$$-\left(\frac{\partial f}{\partial t}\right)_{c\sigma} = -\nu_\sigma\left(f_{\sigma 1} - \frac{n_1}{n_0} f_{\sigma 0}\right) \quad , \tag{4}$$

where ν_σ is the collision frequency of the σ species. This model satisfies the conservation law of particles.

Considering $8\pi nT/B^2 = \beta < (m_e/M_i) << 1$, we neglect magnetic field perturbations so that only the longitudinal response of the plasma to an electrostatic disturbance will be considered:

$$\delta\vec{E} = - \text{grad } \phi \quad . \tag{5}$$

With the longitudinal dielectric constant

$$\varepsilon(\omega,\vec{k}) = 1 + \chi_e + \chi_i \quad , \tag{6}$$

we first derive polarizabilities of electrons and ions as

$$\chi_\sigma = \frac{k_{D\sigma}^2}{k^2}\left\{1 + [\omega+i\nu_\sigma - \omega_\sigma^*(\alpha,\beta_\sigma)]\sum_n \left[\frac{W(z_{n\sigma}) - 1}{\omega+i\nu_\sigma-n\omega_{c\sigma}}\right] I_n(b_\sigma)\exp(-b_\sigma)\right\} \times \left\{1 + i\nu_\sigma \sum_{n=-\infty}^{\infty}\left[\frac{W(z_{n\sigma}) - 1}{\omega-n\omega_{c\sigma}+i\nu_\sigma}\right] I_n(b_\sigma)\exp(-b_\sigma)\right\}^{-1} \tag{7}$$

where

$$\omega_\sigma^*(\alpha,\beta) = \omega_{\sigma n}^*(1+a^*\mu_\sigma) \quad , \qquad \mu_\sigma \equiv \frac{\beta_\sigma}{\alpha} \quad ,$$

$$\omega_{\sigma n}^* = c\,\frac{\alpha T_0}{q_\sigma B}\,k_y \equiv k_y v_{d\sigma}^* \quad , \tag{8b}$$

ω and $\vec{k}$ are wave's angular frequency and propagation vector, and a^* is a correction operator for the temperature gradient; b_σ , z_σ , $W(z)$ are defined conventionally as

$$b_\sigma = \frac{k_y^2 T_\sigma}{m_\sigma \omega_{c\sigma}} = \frac{1}{2} k_y^2 \rho_\sigma^2 \quad , \tag{8c}$$

$$z_{n\sigma} = \frac{\omega + i\nu_\sigma - n\omega_{c\sigma}}{k_z v_e} \quad , \quad v_\sigma = \left(\frac{\kappa T_\sigma}{m}\right)^{-1/2} \quad , \tag{8d}$$

and

$$W(z) = \lim_{\eta \to 0} \frac{1}{(2\pi)^{-1/2}} \int_{-\omega}^{\infty} \frac{te^{-1/2}}{t-z+i\eta} \, dt \quad . \tag{8e}$$

Equation (7) is the most general form of the polarizability which includes electron and ion kinetic and collision effects.

If the wavelength greatly exceeds the mean-free path, kinetic (resonant) effects of particles on waves are suppressed by collisions and simple hydrodynamic approximations are suited to describe the wave phenomena. We shall use the results of earlier works[18,21] for this regime.

A. Low-Frequency Collisional Drift Waves

Considering long wavelength, low-frequency ($\omega << \omega_{ci}$) drift waves for $k_y\rho_e << 1$, $k_y\rho_i < 1$, $\nu_e >> \omega$, $(\omega\nu_e/k_z^2v_e^2) < 1$, and $\omega_{pe} << \omega_{ce}$, the hydrodynamic guiding-center approximations can be used for the calculation of the electron polarizability χ_e since $\lambda_{mfp} << 2\pi/k_z$.[21]

$$\chi_e = \frac{k_e^2}{k^2}\left\{1 + i\cdot 1.44\,\frac{\nu_e}{k_z^2v_e^2}\,[(\omega-k_zu) - \omega_e^*\,(1-0.56\mu_e)]\right\} \tag{9a}$$

$$\text{for} \quad \frac{(\omega-k_zu)}{k_z^2v_e^2} << 1 \quad .$$

Since the parallel electron-thermal-conduction flow is faster than the phase velocity of the wave, the effects of electron thermal and electric conductivity have been included.

For the ion polarizability, in the limit $\omega << \omega_{ci}$, $(\omega/k_zv_i) >> 1$, $b_i << 1$, and $\mu_i << 1$, using Eq. (7),

$$\chi_i = \frac{k_{Di}^2}{k^2}\left\{\frac{\omega_i^*(1-b) + \omega b_i + i\nu_\perp}{\omega + i\nu_\perp}\right\} \quad , \tag{9b}$$

where $\nu_\perp = b_i \nu_{ii} = \frac{1}{2}k_\perp^2 \rho_i^2 \nu_{ii} << \omega$ is an effective ion collision frequency.

Substituting the experimental conditions, $T_{eo} = T_{io}$, $b_i < 1$ and $\mu_i << 1$, into Eqs. (9a) and (9b), one obtains wave frequency and growth rate:

$$\omega_R = \text{Real } (\omega) = \omega_e^* (1-2b_i) \quad , \tag{10a}$$

$$\gamma \simeq \text{Im}(\omega) \simeq 1.44\ \omega_e^* \left\{\frac{[k_z u + \omega_e^*(2b-0.56\mu_e)]}{k_z^2 v_e^2}\right\} - \nu_\perp \quad . \tag{10b}$$

These results resemble those obtained by Ellis and Motley[11] except that we include effects of perpendicular electron-temperature gradients, present whenever electron current is drawn through Q-machine plasmas. Note that the negative radial temperature-gradient ($\mu_e < 0$) produced by the current contributes to the destabilization of this wave. Since most of the hydrodynamic aspects of current-driven low-frequency drift waves are well documented,[11] we do not discuss details of this instability. However, this current-driven drift wave has higher growth rate than the similar non-current-driven drift wave and thus produces strong anomalous particle diffusion.

B. Ion-Cyclotron Drift Wave (Discrete spectrum)

As the drift wave frequency $(\omega^*_{i,e})$ is increased to the vicinity of ω_{ci}, we expect coupling between drift and electrostatic ion-cyclotron waves. Both drift and cyclotron modes propagate predominantly perpendicular to the magnetic field, and thus couple effectively.[22,23,24]

In the present experiment the electrostatic ion-cyclotron wave can be excited by resonant (inverse Landau damping) interaction between electron current and wave. Furthermore, free energy from the spatial inhomogeneity may be tapped, resulting in diamagnetic-drift ion-cyclotron instabilities. Depending on k_z, different modes may occur, which will now be discussed.

1. Short Parallel Wavelength, $k_z \neq 0$

We first consider the electrostatic ion-cyclotron drift wave with discrete spectrum for $|\omega+i\nu_e| < k_z v_e$. Since $\nu_e < k_z v_e$ is satisfied in the low-density regime, electron collision effects can be neglected and the electron polarizability can be easily derived for $\omega << \omega_{ce}$ from Eq. (7)

$$\chi_e = -\frac{k_{De}^2}{k^2}\left\{1 + i\left(\frac{\pi}{2}\right)^{1/2}\frac{\omega - k_z u - \omega_e^*(1-\mu_e/2)}{|k_z| v_e}\right\} . \quad (11)$$

The ion polarizability is expressed (for $\nabla T_i = 0$) as

$$\chi_i = \frac{k_{Di}^2}{k^2}\left(1 - \sum_n \left(\frac{\omega+i\nu_i-\omega_i^*}{\omega+i\nu_i-n\omega_{ci}}\right) I_n(b_i)\exp(-b_i)\left\{1-i\left(\frac{\pi}{2}\right)^{1/2}\left(\frac{\omega-n\omega_{ci}}{k_z v_i}\right)\right.\right.$$

$$\left.\left.\times \exp\left[-\frac{(\omega-n\omega_{ci})^2}{2k_z^2 v_i^2}\right]\right\}\right)\times\left\{1 - i\nu_i \sum_n \left[\frac{I_n(b_i)\exp(-b_i)}{\omega+i\nu_i-n\omega_{ci}}\right]\right\}^{-1} , \qquad (12)$$

where we have utilized $\omega-n\omega_{ci} > k_z v_i$, ν_i .

From the real part of $\varepsilon(\omega,\vec{k}) = 1 + \text{Re}\,\chi_c + \text{Re}\,\chi_i$ we obtain a general dispersion relation for ion-cyclotron drift modes:

$$1 + \frac{k_{De}^2}{k^2} + \frac{k_{Di}^2}{k^2}\left[1 - \frac{\omega-\omega_i^*}{\omega} f_\omega(b_i)\right] = 0 , \qquad (13a)$$

where

$$f_\omega(b_i) \equiv \sum_{n=-\infty}^{\infty} \frac{\omega}{\omega-n\omega_{ci}} I_n(b_i)\exp(-b_i) . \qquad (13b)$$

If the frequency approaches $\omega \simeq n\omega_{ci}$,

$$\omega = n\omega_{ci}\left[1 + \frac{T_e}{T_i+q(b_i)T_e} I_n(b_i)\exp(-b_i)\left(1 - \frac{k_y v_{di}^*}{n\omega_{ci}}\right)\right] , \qquad (14)$$

where v_{di}^* is the ion-diamagnetic drift velocity due to the plasma density inhomogeneity; an ion-temperature correction factor $q(b_i)$ approaches 0 for $b_i \ll 1$ and 1 for $b_i \gg 1$. For $v_{di}^* = 0$ and $q(b_i) \ll 1$, we recover the dispersion relation of Drummond and Rosenbluth[14] for the ion-cyclotron wave in a homogeneous plasma.

When ω_i^* , $\omega_e^* \ll n\omega_{ci}$, the threshold parallel electron drift velocity u necessary for the destabilization of this

instability can be derived by invoking $\gamma = -\mathrm{Im}\varepsilon/(\partial\varepsilon_r/\partial\omega) > 0$. Drummond and Rosenbluth[14] calculated the threshold value of u for hydrogen plasmas with $\omega_i^* = \omega_e^* = 0$, $\nu_i = 0$ and $q(b_i) << 1$. If viscosity is included, the threshold value of u is

$$\left(\frac{u}{v_i}\right)_{thr} \simeq 2\sqrt{2}\left(1 + \frac{T_i}{T_e}\frac{1}{\Lambda_n}\right)\left[\ell n\left\{\left(\frac{m_i}{m_e}\right)^{1/2}\left(\frac{T_e}{T_i}\right)^{3/2}\Lambda_n\right\}\right]^{1/2}$$

$$+ \left(\frac{2}{\pi}\right)^{1/2}\frac{1}{n\omega_{ci}\tau_i}\left(\frac{m_i}{m_e}\right)^{1/2}\left(\frac{T_i}{T_e}\right)^{1/2}\frac{1-\Lambda_n}{\Lambda_n} \qquad (15a)$$

where $\Lambda_n = I_n(b_i)\exp(-b_i)$. The second term on the right side in Eq. (15a) is due to ion viscosity. For $n = 1$, $T_i \simeq T_e$, $m_i/m_e = 8\times10^4$ (potassium), the minimum value for $(u/v_i)_{thr}$ is

$$\left(\frac{u}{v_i}\right)_{min} \simeq 30\left(1 + \frac{26}{\omega_{ci}\tau_i}\right) . \qquad (15b)$$

It is noteworthy that ion viscosity comes into play even for $\omega_{ci}\tau_i >> 1$.[25] However, it can be neglected in the calculation for the present ion-cyclotron waves except for the high-density regime, $n_e > 10^{11}\mathrm{cm}^{-3}$.

Including effects of diamagnetic current due to the plasma inhomogeneity (v_{di}^*, v_{de}^*), the growth rate can be expressed as

$$\gamma = \left(\frac{\pi}{2}\right)^{1/2}(n\omega_{ci}-\omega_i^*)\frac{T_e}{T_i}\Lambda_n\left[\frac{k_z u+\omega_e^*(1-\mu_e/2)-\omega}{k_z v_e}\right.$$

$$\left. - \frac{T_e}{T_i}\Lambda_n\frac{n\omega_{ci}-\omega_i^*}{k_z v_i}\exp\left(\frac{-\Delta^2}{2k_z^2 v_i^2}\right)\right] \qquad (16)$$

where $\Delta = \omega - n\omega_{ci}$.

From Eq. (16) one concludes that for $\omega_{ci} > \omega_i^*$, this instability with discrete spectrum ($\omega \simeq n\omega_{ci}$) is driven mainly by the parallel electron current ($n_e eu$) and its threshold value decreases when the wave propagates in the direction of the electron diamagnetic drift. Recently, Hudson[26] investigated the finite, parallel heat-conductivity effect on this mode and found it increases the threshold in the limit $(k_z^2 v_e^2/\omega\nu_e) >> 1$. For $\omega_i^* > \omega_{ci}$, the instability can be driven by free energy from the plasma inhomogeneity. Electron current stabilizes the instability under this condition.

2. Long Parallel Wavelength, $k_z \simeq 0$

Next, we investigate instabilities with long parallel wavelength: The parallel phase velocity of the wave is much larger than the electron-thermal velocity, so that there is no resonant interaction between parallel electron current and wave. Thus, instability is possible only when the free energy of the plasma inhomogeneity (pressure gradients) can be fed into the wave.[22,24] We neglect terms containing $k_z u$, since $k_z \simeq 0$ and $u << v_e$ in the experiment.

For $\omega > \nu_e$ and $\omega_{ce} >> \omega_{pe}$, the electron polarizability for this condition is derived from Eq. (7) as

$$\chi_e = \frac{k_{De}^2}{k^2}\left\{\frac{\omega_e^*}{\omega} - \frac{k_z^2 v_e^2}{\omega^2}\left[1 - \frac{\omega_e^*}{\omega}(1+\mu_e)\right] + i\frac{\nu_e}{\omega}\frac{k_z^2 v_e^2}{\omega^2}\left[1 - \frac{\omega_e^*(1-\mu_e/2)}{\omega}\right]\right.$$

$$\left. + i\left(\frac{\pi}{2}\right)^{1/2}\frac{\omega-\omega_e^*[1+\mu_e(\omega^2/2k_z^2v_e^2)]}{k_z v_e}\exp\left(\frac{-\omega^2}{2k_z^2v_e^2}\right)\right\} . \quad (17a)$$

For $\omega < \nu_e$, the dominating term in the kinetic equation (Eq. 3) is the collision term. In this regime hydrodynamic approximations or kinetic equations with the aid of the Chapman-Enskog method should be used (see Rukhadze and Silin[18]). Both methods yield the same result:

$$\chi_e = \frac{k_{De}^2}{k^2}\left\{\frac{\omega_e^*}{\omega} + i\,1.96\,\frac{k_z^2 v_e^2}{\omega\nu_e}\left[1 - \frac{\omega_e^*}{\omega}(1+1.71\mu_e)\right]\right\} \quad . \tag{17b}$$

The ion polarizability is the same as that of Eq. (12); ion-cyclotron damping is negligible, for $k_z \simeq 0$.

For $\omega \simeq n\omega_{ci}$, the ion polarizability is

$$\chi_i = \frac{k_{Di}^2}{k^2}\left\{1 - \frac{\omega - \omega_i^*[1+b_i\mu_i(\partial/\partial b_i)]}{\omega - n\omega_{ci}}\Lambda_n(b_i)\right\} \quad . \tag{18}$$

Thus, solving the dispersion relation, $1 + \chi_e + \chi_i = 0$, with $\mu_i \simeq 0$, we obtain the oscillation frequency:

$$\left.\begin{aligned} \omega_1 &\simeq \frac{\omega_i^*}{1 + k^2\lambda_{Di}^2} \quad , \\ \text{or} \qquad \omega_2 &\simeq n\omega_{ci}\left\{1 + \frac{[1-(\omega_i^*/n\omega_{ci})]\Lambda_n}{k^2\lambda_{Di}^2 - (\omega_i^*/n\omega_{ci})}\right\} . \end{aligned}\right\} \tag{19}$$

Mikhailovskii and Timofeev[22] predicted that the latter mode with $\omega \simeq n\omega_{ci}$ results in the "drift cyclotron instability," which has been conclusively identified in the recent experiment.[24] Neglecting ion and electron temperature gradients in Eq. (17a,b) and (18), we recover their stability criterion,

$$\alpha \rho_i > 2 \frac{\omega_{ci}}{\omega_{pi}} \quad , \tag{20}$$

where

$$\alpha = \frac{1}{n_e} \frac{dn_e}{dx} \quad .$$

Examining the imaginary part of χ_e and χ_i, we conclude that both negative electron-temperature gradient $[d(\ell n\, T_e)/d(\ell n\, n_e) < 0]$ and positive ion-temperature gradient $[d(\ell n\, T_i)/d(\ell n\, n_i) > 0]$ contribute to the destabilization of the wave. Note that the above criterion was obtained for the flute mode $(k_z = 0)$ without considering ion-collisional damping: Unless $\omega - n\omega_{ci} >> \nu_{ii} k_\perp^2 \rho_i^2$, instability cannot occur even when Eq. (20) is satisfied.

C. High-Frequency Drift Wave (Ion-Cyclotron Drift Wave with Continuous Spectrum; $\omega \gtrsim \omega_{ci}$)

Drift cyclotron instabilities may occur in the frequency region $|\omega - n\omega_{ci}| >> \nu_{ii} k_\perp^2 \rho_i^2$, $k_z v_i$, if they can overcome effective collisional and ion-cyclotron damping. With $k_\perp^2 \rho_i^2 >> 1$, for ion-cyclotron drift waves, one can expect destabilization of waves with frequencies far from the ion-cyclotron frequency. In comparison with the previous case where unstable modes exist only around $\omega \simeq n\omega_{ci}$, we now expect unstable waves continuously covering a wide frequency range $(\Delta\omega > \omega_{ci})$. We call this mode "ion-cyclotron drift wave with continuous spectrum," or "high-frequency drift wave." Mikhailovskii predicted[23] this high-frequency instability with $k_z = 0$ for a strongly inhomogeneous plasma which satisfies the condition $\alpha\rho_i > (m_e/m_i)^{1/4} [1/(1 + \omega_{ce}^2/\omega_{pe}^2)]$. Under this condition one expects a high-frequency drift wave with continuous spectrum $(\omega \gtrsim \omega_{ci}$, $\gamma \simeq \omega_{ci})$.

1. Short Parallel Wavelength, $k_z \neq 0$

Consider high-frequency drift waves with finite parallel wavelength $(\omega/k_z v_e < 1 \ , \ \omega/\omega_{ci} > 1)$. From Eq. (7), we write the polarizabilities of electrons and ions

$$\left.\begin{aligned} \chi_e &= \frac{k_e^2}{k^2}\left[1+i\left(\frac{\pi}{2}\right)^{1/2}\frac{\omega - k_z u - \omega_e^*(1-\mu_e/2)}{k_z v_e}\right] \\ \text{and} \qquad \chi_i &= \frac{k_i^2}{k^2}\left[1 - (1 - \frac{\omega_i^*}{\omega})\ f_\omega(b_z)\right] \quad , \end{aligned}\right\} \tag{21}$$

where ion-cyclotron damping is neglected $[(\omega-n\omega_{ci})/k_z v_i >> 1]$. A general solution for the dispersion relation can be stated as

$$\omega = \frac{-\omega_i^* f_\omega(b_i)}{[1-f_\omega(b_i)] + (T_i/T_e)\ [1 + i\ \mathrm{Im}\ \chi_e(\omega,k)] + k^2\lambda_{Di}^2} \ , \tag{22}$$

with an asymptotic form[27] $f_\omega(b_i)$ for $b_i >> 1$ and $\omega/\omega_{ci} >> 1$

$$f_\omega(b_i) \simeq \xi Z_r(-\xi) + i\xi(\cot\frac{\omega}{\omega_{ci}})\ \sqrt{\pi}\ \exp(-\xi^2) \quad , \tag{23}$$

where $\xi = \omega/\sqrt{2}k_y v_i$, and Z_r is the real part of the plasma dispersion function,[28] $Z(\xi) = [W(\sqrt{2}\xi) - 1]/\xi$. Since $0 \leq f_\omega(b_i) \leq 1$, the wave with finite parallel wavelength $(\omega/k_z < v_e)$ propagates predominantly in the direction of the electron diamagnetic drift. For instance, for $\xi > 1$ and $k^2\lambda_{Di}^2 << 1$,

$$\omega \simeq \omega_e^* \left\{ 1 + i\left(\frac{\pi}{2}\right)^{1/2} \left[\frac{k_z u - \frac{1}{2}\mu_e \omega_e^*}{k_z v_e} - \frac{\omega_e^* [1+(T_e/T_i)]}{k_y v_i} \exp\left(-\omega^2/2k_y^2 v_i^2\right) \right] \right\} . \tag{24}$$

From Eq. (22) we conclude that parallel electron drift and negative electron-temperature gradient ($dT_e/dn_e < 0$) contribute to the destabilization of the wave.

Taking the limit $\omega_i^* , \omega_e^* \to 0$ and $\omega/\omega_{ci} >> 1$, $k_y \rho_i >> 1$, we obtain the dispersion relation of ion sound in the non-magnetized plasma, as expected:

$$1 + \frac{k_{De}^2}{k^2}\left(1+i\sqrt{\frac{\pi}{2}}\,\frac{\omega - k_z u}{k_z v_e}\right) - \frac{\omega_{pi}^2}{\omega^2} + i\,\frac{k_{Di}^2}{k^2}\sqrt{\frac{\pi}{2}}\,\frac{\omega}{k v_i}\exp\left(-\omega^2/2k^2 v_i^2\right) = 0 . \tag{25}$$

2. Long Parallel Wavelength, $\omega > k_z v_e$

Finally, we examine flute modes ($k_z \simeq 0$) with continuous spectrum in the regime $\omega \neq \omega_{ci}$, $b_i >> 1$ and $\nu_e > \omega$. The dispersion relation is obtained from Eq. (7):

$$1 + \frac{k_{De}^2}{k^2}\left\{\frac{\omega_e^*}{\omega} + i\,1.96\,\frac{k_z^2 v_e^2}{\omega \nu_e}\left[1 - \frac{\omega_e^*}{\omega}\left(1+1.71\mu_e\right)\right]\right\}$$

$$+ \frac{k_{Di}^2}{k^2}\left\{1 - \left[1 - \frac{\omega_i^*[1+\mu_i T_i(\partial/\partial T_i)]}{\omega}\right] f_\omega(b_i)\right\} = 0 . \tag{26}$$

For $\omega/\omega_{ci} >> 1$ and $\gamma = \mathrm{Im}\,\omega > \omega_{ci}$, an asymptotic form of $f_\omega(b_i)$ results in

$$f_\omega(b_i) \simeq -\xi \cdot Z_r(\xi) + i\sqrt{\pi}\xi \exp(-\xi^2) \quad , \tag{27}$$

where $\xi = \frac{1}{\sqrt{2}} \frac{\omega}{k_y v_i}$.

Substituting Eq. (27) into (26), one obtains the frequencies:

$$\omega \simeq \frac{\omega_i^*}{1 + k^2 \lambda_{Di}^2} \qquad \text{for} \quad \frac{\omega}{k_y v_i} < 1 \quad , \tag{28}$$

or $$\omega \simeq \frac{\omega_i^*}{1 - (\omega/\omega_{pi})^2} \qquad \text{for} \quad \frac{\omega}{k_y v_i} > 1 \quad . \tag{29}$$

Thus, we conclude that ion-cyclotron drift waves with continuous spectrum and long parallel wavelength ($\omega > k_z v_e$) propagate predominantly in the direction of the ion-diamagnetic drift velocity (due only to density and not temperature gradient). The growth rate, however, is affected by the temperature gradients of electrons and ions. For example, in the case of $\omega/k_y < v_i$,

$$\gamma \simeq \frac{T_i}{T_e} \omega_i^* \left\{ - 1.96 \frac{k_z^2 v_e^2}{\omega_i^* \nu_e} \left[1 + \frac{T_e}{T_i} (1 + 1.71\mu_e) \right] \right.$$

$$\left. - \left(\frac{\pi}{2}\right)^{1/2} \frac{T_e}{T_i} \frac{\omega_i^*}{2kv_i} \mu_i \right\} - \nu_\perp \quad , \tag{30}$$

where the last term $\nu_\perp \simeq \frac{1}{2} k_\perp^2 \rho_i^2 \nu_{ii}$ denotes viscosity damping.

Thus, a negative temperature gradient of electrons or ions can destabilize the continuous-spectrum instability with high growth rate ($\gamma \lesssim \omega_{ci}$) .

In conclusion, when $|\omega^*_{i,e}| < \omega$, instabilities can only be excited by resonant interaction between the parallel electron current (with $\omega/k_z v_e < u < v_e$) and the wave. For $|\omega^*_{i,e}| > n\omega_{ci}$, drift waves with discrete or continuous frequency spectrum up to $n\omega_{ci}$ can be destabilized due to the plasma inhomogeneity. The negative temperature gradient of electrons and ions (μ_e, $\mu_i < 0$) , produced by parallel electron current in the experiment, can generate unstable, continuous-spectrum, high-frequency drift waves and dominates the stability of the system.

III. EXPERIMENTAL APPARATUS AND TECHNIQUES

The experiments were performed on the Princeton Q-1 thermally ionized plasma, Fig. 1. Plasma is produced by surface ionization of neutral alkali metal atoms on hot tungsten ionizers, which simultaneously emit the neutralizing thermionic electrons. These ionizer (end) plates are 3.2 cm in diameter and placed perpendicularly to the magnetic flux, 125 cm apart, thus defining the radial and axial extent of the plasma column. Four beams of neutrals impinge on each ionizer plate, so that the resulting plasma column is axisymmetric with no net drift along the axis, in equilibrium. The confining magnetic field (up to 7 kG) is spatially and temporally constant, with a deviation of less than 0.3%.

The residual, neutral pressure during operation is $< 10^{-7}$ Torr, giving a mean-free path for ion-neutral collisions of about 50 m. The device is operated in the electron-rich condition, with electron emission much higher than ion emission. The plasma charges up negatively, to repel electrons, and the ions are electrostatically confined. However, electrons are in good contact with the end plates. Ion confinement times are about 5 msec and electron confinement times are orders of magnitude shorter. Current is applied through the end plates, parallel to B. Twenty different port holes are available to locate radially movable probes. An axially movable probe can traverse one half of the length of the plasma column, at any desired radial position. The following diagnostics are used:

n_e , n_i : Langmuir probes (ion saturation current, locally) and microwave cavity (weighted average radially). The cavity checks probe accuracy in the presence of fluctuating and steady-state electric fields.

T_e : Langmuir probes.

T_i : Perpendicular ion temperatures (assumed equal to parallel T_i at experimental conditions, due to high ion-ion collision frequency relative to ion life time) were determined using special (Langmuir) probes with mechanical limiter prohibiting electron collection.[29] These probes have been independently calibrated by optical and diamagnetic loop temperature measurements.

u : Rotating plane Langmuir probes, which can be turned into or away from the electron drift, thus giving precise, local drift velocity measurements, $j = n_e(\frac{1}{4} v_{the} \pm u)$. The same probe characteristic is used to obtain u , v_{the} , and n_e .

ϕ : From probe floating potential, corrected for detailed dependence of ion saturation current on density.

$\tilde{n}$, $\tilde{\phi}$: $\tilde{n}$ from oscillatory part of probe ion saturation current, and, for the higher frequency measurements, from electron current fluctuation of 50 Ω matched probes. For ϕ measurements high impedance probes were used.

ω : Doppler-shift due to $E \times B$ rotation of the plasma resulting from radial electric fields was taken into account in determination of instability frequencies.

γ : From oscillograms of time evolution of instability in pulsed operation, both during onset and decay.

$k_\perp$: Rotating double probe, with separation of probe tips comparable to perpendicular wavelength. When the separation of the probe tips is comparable to the wavelength, the phase shift upon rotation can be used to determine wavelength.

$k_\parallel$: Determined with two probes separated 2 cm to 30 cm and carefully aligned parallel to B.

η : From (external) I-V characteristic, or locally by immersion-type, electrodeless rf conductivity probe, ($f < 0.5$ MHz) based on the dissipation seen by a marginal-oscillator test coil.[30,31] Since the resonance frequency of this probe is much smaller than the electron-ion collision frequency ν_{e-i}, the dc conductivity of the plasma is obtained. Results from this probe are local ($\approx$1 cm) in terms of the axial extent of the plasma but do not give good radial resolution. (The axial diffusion time for electrons over the machine length is much greater than the rf period.)

In regard to the ion heating measurements, we note that the electron-ion relaxation time is much longer than the ion confinement time, so that ohmic heating of the ions is negligible in these plasmas. Concerning the resistivity measurements, since electron collisional ionization does not take place (low T_e) and the residual pressure is low, there can be no impurity ions present; thus, any increase in resistivity cannot be due to multiply charged impurity ions, as may be the case in Tokamaks.

IV. EXPERIMENTAL RESULTS

A. Evolution of Instabilities and Anomalous Effects

Increasing the plasma current causes successive destabilization of four different instabilities, which generate specific effects on the plasma parameters, as shown in Table 1. For low currents, the measured resistivity is in agreement with the Spitzer-Härm value, since sheath resistance at the end plates can be neglected for $n_e > 10^{10} cm^{-3}$.[6] The small amount of electron heating observed in this regime leads to slight reduction of resistivity with increased electron drift velocity, as expected. Note that the electron current produces the negative (radial) shear of drift velocity and electron temperature, as expected from $\eta_{class}(r) = \text{const.}$ and $j(r) = n_e(r)eu(r) = \text{const.}$: Fig. 1. The classical-resistivity, (electron) ohmic-heating regime is characterized in the I-V plot by the nearly straight line near the origin, Fig. 2.

For $u \simeq 5\ v_{thi}$, the current-driven collisional drift wave becomes unstable with a frequency $f \simeq 3$ kHz . This instability is well understood and has been described in detail before.[11] Coincident with its onset, density reduction due to the radial transport caused by the drift wave occurs.[32] There is no observable change of the resistivity; although we have carefully searched for effects on the resistivity with onset (which might also give a clue on the energy flow from parallel electron motion into the instability), no change could be detected (± 0.3%). Thus, the onset of the collisional drift instability does not affect the I-V characteristic.

For $u \simeq 30\ v_{thi}$ $(0.1\ v_{the})$, an ion-cyclotron wave is destabilized, with $\omega \simeq 1.14\ \omega_{ci}$. This instability was

identified as the discrete-spectrum ion-cyclotron drift wave.[16] It generates a small amount of anomalous resistivity ($\simeq$10%) and ion heating ($\approx$200%). Rynn et al.[33] observed similar ion heating induced by electrostatic ion-cyclotron waves excited by an electron current in the central part of Q-device plasmas, in which no diamagnetic-drift effects exist.

Increasing the electron drift velocity to $\approx 0.2\ v_{the}$ excites the continuous-spectrum high-frequency drift wave, $\omega_{ci} < \omega < \omega_{pi}$, and results in anomalous resistivity an order of magnitude above the initial resistivity and in intense ion heating ($\simeq 10\ T_{i0}$).[17] Note that η_{anom}/η_{class} has increased by a much larger factor since the ohmic current has decreased the classical resistivity ($T_e/T_{e0} \simeq 3$). This large increase in resistivity leads to current inhibition, the most remarkable effect in the I-V characteristic, Fig. 2. After reaching current inhibition, the current never approaches the previous maximum value again, even for much higher applied voltages. Thus, we observe a large increase in resistivity coincident with the onset of a continuous-spectrum ion-sound-like drift wave (a) for an increase in electron temperature (which should reduce the resistivity), (b) in a fully ionized plasma (where resistivity is nearly independent of density), and (c) in a plasma which is free of multiply ionized impurities (which could increase resistivity).

For $u = 1/3\ v_{the}$, a high-frequency electron instability is destabilized. This instability has a frequency

$f = 30 - 300$ MHz $= 5\ f_{pi} - \frac{1}{10}\ f_{pe}$, and is very effective in heating the electrons and in reducing the radial electron temperature gradient that existed for lower electron drift velocities. The electron drift velocity is found to saturate at $\frac{1}{3}\ v_{the}$.

B. Identification of Instabilities

In this section we present detailed identifications of the different instabilities excited by electron current directly or indirectly in our isothermal inhomogeneous plasma.

1. Low-Frequency Collisional Drift Wave (LFDW):

When the electron current reaches $u/v_i \simeq 5$, low-frequency collisional drift waves with discrete spectrum ($\omega/2\pi \simeq 3$KHz) develop ($\tilde{n}/n_{eo} \lesssim 30\%$). Since Ellis and Motley[11] have reported extensive measurements on this current-driven LFDW and its perpendicular structure is similar to the current-free drift mode,[34] we limit our discussion to the following few remarks.

According to Eqs. (10a) and (10b), the instability occurs when the destabilizing effects of parallel electron current and negative temperature-gradient overcome ion-viscosity damping. In the high-density regime ($n_{eo} > 10^{10}$ cm^{-3}), the wave is stable without current for low magnetic fields. Thus, one can observe the onset of oscillations and the resultant density decrease. In the low-density regime $n_{eo} \lesssim 10^{10}$, the wave is unstable even without current.[35] However, the wave amplitude grows from $(\tilde{n}/n_{eo})_{max} \simeq 0.1$ to $(\tilde{n}/n_{eo})_{max} \simeq 0.3$ when electron current is drawn along the axis, and the current-driven drift waves generate more radial transport than non-current-driven drift waves.[11]

2. Ion-Cyclotron Drift Wave with Discrete Spectrum (ICDW):

As the electron current along B is raised so that $u \simeq v_e/10$, a wave with discrete frequency $\omega \simeq 1.14\ \omega_{ci}$ destabilizes in agreement with the prediction of Section II, (Fig. 3). Because the electron current density is constant with respect to radius [$E(r) = \text{const}$, $\sigma(r) \simeq \text{const}$; thus, $j(r) \simeq \text{const}$], the parallel electron drift velocity, $u = j/n(r)e$, reaches the threshold value for destabilization of the wave first at the outer radius of the column, where the plasma density $n(r)$ is lower. Thus, we observe that the instability first appears at the periphery of the plasma and then spreads into the center of the column as the applied, steady-state voltage is increased.

The azimuthal phase velocity was measured to be in the direction of the ion-diamagnetic drift and $k_y\rho_i \simeq 1.5$. Near onset, $\omega_i^* \ll \omega_{ci}$, and inhomogeneous plasma effects are small; thus, the discrete wave is similar to the electrostatic ICW first observed by D'Angelo and Motley[36] and theoretically explained by Drummond and Rosenbluth.[14] However, two characteristics of drift waves are present: (1) the wave propagates azimuthally, parallel to the ion-diamagnetic drift (opposite to the E×B drift), and (2) the oscillation frequency is reduced at the periphery of the plasma column (12 mm) and increases with v_{ext}, as seen in Fig. 4. The latter characteristic is predicted by the ICDW dispersion relation [Eq.(14)] of Section II. We note that

Doppler-effect due to plasma rotation can be neglected in this region.

Spatial growth of the wave was observed ($\approx$0.5 to 1 dB/cm). The parallel phase velocity was measured to be $\omega/k_z \approx u/2$,[14] indicating excitation by the parallel current.

Equation (16) predicts ion-cyclotron drift waves which propagate parallel to the electron diamagnetic drift and should destabilize at low parallel electron drift. However, we did not observe this mode.

3. High-Frequency Drift Wave (Ion-Cyclotron Drift Wave with Continuous Spectrum):

When the electron current is increased further after destabilization of the discrete spectrum ICDW, a higher frequency instability with continuous spectrum and maximum fluctuation amplitude at $\omega_{peak} \approx 1/3\ \omega_{pi} >> \omega_{ci}$ sets in. The frequency of this amplitude maximum changes proportional to $\sqrt{n_e}$. This feature of the wave is similar to that of an ion acoustic wave, but measurements of parallel electron drift velocity ($u/v_e \lesssim 0.3$) throughout the plasma indicate that the ion acoustic wave should be stable for the measured temperature ratio, $T_e/T_i < 1$.

This paradox was resolved by measurements of parallel and perpendicular wavelengths. It was found that the wave propagates predominantly azimuthally ($k_y >> k_x >> k_z$), with the ion-diamagnetic drift velocity.

Figure 5a displays the measured dispersion relation of the high-frequency drift wave with continuous spectrum for constant magnetic field and applied voltage. The solid line is $\omega/k_y = v_{di}^*$, calculated from the static plasma parameters. Figure 5b shows measured azimuthal phase velocity as a function of B. The solid line is again $v_{di}^* = cT_i\alpha/eB$. The parallel wavelength was measured to be comparable to the machine length, indicating $\omega/k_z > v_e$. These measurements thus demonstrate that this instability with continuous spectrum is a diamagnetic drift wave, as predicted for $\omega_i^* > \omega_{ci}$ and $\alpha\rho_i > 2\omega_{ci}/\omega_{pi}$.[22] The measured dispersion relation agrees with Eq. (28), $\omega/k_z > v_e$, and the essential condition for destabilization, $\mu_e \lesssim -1$, is satisfied in the experiment.

Furthermore, in the steady-state experiment, the negative ion temperature profile ($\mu_i < 0$) is obtained by the effect of discrete ICDW, which in turn increases the growth rate of the continuous ICDW.

Thus, contrary to the discrete ICDW,[22] this high-frequency drift wave with continuous spectrum is driven by negative temperature gradients produced by parallel electron current in the radially inhomogeneous plasma, as predicted by Eq. (30).

To investigate the time-dependent behavior of the instability, we pulsed the parallel electron current. As seen in Fig. 6, the wave grows first at the periphery of the column where higher parallel drift velocity and higher negative temperature gradient are present.

Azimuthal and parallel propagation of this wave in pulsed operation was more complicated than in steady state. In slow-pulse operations ($1/I \cdot dI/dt \lesssim 10^4$/sec) the wave features were similar to those of steady-state experiments, but in fast-pulse operation the discrete spectrum ICDW was not observed, confirming that the continuous ICDW is not a nonlinear stage of the discrete instability.

4. High-Frequency Electron Wave:

Finally, high frequency, $\omega_{pi} << \omega << \omega_{pe}$, electron waves with broad spectrum ($\omega_{peak} \simeq 60$ MHz ~ 200 MHz) were observed when the applied voltage was raised far above the current inhibition in the I-V characteristic. Measurements of the perpendicular propagation indicated standing waves; parallel wavelength could not be measured accurately. Gould-Trivelpiece modes are eigenmodes of the Q-device plasma and can be expected to fall into the same frequency range. Based on the appearance of a bump in the tail of the electron distribution function (measured by parallel electron energy analyzer), this high-frequency wave has been considered to be a Gould-Trivelpiece[37] mode driven by the fast component of the electron stream along the axis. A more conclusive identification of this wave is yet to be done.

C. Anomalous Plasma Parameters

Coincident with the onset of the four instabilities discussed, we observe various anomalies in the plasma such as enhanced radial diffusion, enhanced resistivity and particle heating, and anomalous electron thermal conductivity and viscosity. We now describe those anomalies in detail except for enhanced diffusion, which has already been investigated[11,32] for similar conditions.

1. Resistivity:

Measured resistivities, for small currents, agree with the classical (Spitzer-Härm) value, when sheath resistances at the end plates can be neglected ($n > 10^{10}$ cm^{-3}) .[6]

Onset of the collisional drift wave does not change the plasma resistivity and the ion-cyclotron drift wave with discrete spectrum produces only a small enhancement of the resistivity (Fig. 3). This small increase (10~20%) was predicted by Bers et al.[38] and agreed with our calculation in Ref. 17. As the high-frequency drift wave (continuous-spectrum ICDW) becomes dominant, the resistivity changes by an order of magnitude and current inhibition sets in, as seen from the I-V curve of Fig. 2.

However, resistivity measurements from I-V curves cannot be considered conclusive since the sheath resistances in front of the end plate might play an important role after onset of

instabilities. To measure internal (or local) parallel resistance of the plasma, an immersion-type electrodeless rf conductivity probe[30,31] was used, based on the dissipation seen by a marginal oscillator test coil (Fig. 7). The coil is shielded electrostatically and kept at constant temperature during the measurements; the coil temperature is monitored by a thermistor (Fig. 7). Since the resonance frequency of this probe ($f_o < 0.5$ MHz) is much smaller than the electron-ion collision frequency ν_{e-i}, this probe determines parallel DC conductivity; $\sigma \simeq ne^2/m_e\nu_{ei}$.

In Fig. 8, the conductivity (relative value) measured by the rf probe is compared with the I-V conductivity in steady-state operation. To measure time dependence of the ICDW amplitude and plasma resistance, we performed a pulsed experiment applying sawtooth-shape voltage to the plasma. Figure 9 shows conductivity measured by the rf probe, density fluctuations of the continuous ICDW, and total electron current and V_{appl} with respect to time. Coincident with onset of instability, one observes a reduction of conductivity in both the rf probe signal and plasma I-V curve.

The data from the I-V curve and rf probe agree with each other within 50% error for $V_{appl} < 5V$, $n_e > 10^{10}$ cm^{-3}, indicating that the conductivity determined from the I-V curve is the correct plasma conductivity, except for $E_{appl} > E_{runaway}$ or $n_e < 10^{10}$ cm^{-3}. The rf probe geometry is considered to be more sensitive to parallel than

perpendicular conductivity since $\sigma_{\parallel} > \sigma_{\perp}$. The anomaly in perpendicular resistivity is expected to be stronger, but was not measured explicitly.

In Fig. 10a, normalized parallel electron drift velocity and onset points of the three different instabilities are plotted with respect to applied voltage. Saturation of electron drift occurs after the amplitude of the continuous-spectrum ICDW saturates and before onset of the high-frequency electron wave. Figure 10b shows that rapid increase of normalized resistivity occurs with saturation of the drift velocity.

2. Heating:

In the steady-state experiment, a moderate increase of ion temperature is observed coincidental with onset of the discrete ICDW $(T_i/T_{io} \simeq 3)$. As the continuous-spectrum ICDW becomes dominant with increased applied voltage, T_i increases greatly to a few eV $(T_i/T_{io} \simeq 10)$ and saturates. This increase of ion temperature must be considered a result of wave heating, since the electron-ion relaxation time is much longer than the ion confinement time, so that ohmic heating of ions can be neglected.

The mechanism of energy transfer is the following. For the discrete ICDW, the parallel electron drift energy is converted into wave energy through inverse Landau damping, and from wave to ion energy through cyclotron damping. Thus, parallel electron kinetic energy is

transferred into (perpendicular) ion thermal energy. For the continuous-spectrum ICDW, free energy from the plasma inhomogeneity ($\nabla_r n_e$; $\nabla_r T_e$, due to current) contributes to the destabilization of the wave, and the wave energy is then converted into ion thermal energy through ion Landau damping ($k_\perp \rho_i >> 1$) .

To obtain additional data and to measure the time scale of wave heating, we performed pulsed experiments. In Fig. 11, from top to bottom, applied voltage, total current, fluctuation amplitude of the continuous ICDW, and normalized ion-temperature are plotted with respect to time. We observe that the heating time of the ions (τ_h ; $1/\tau_h \simeq 1/T_i \cdot dT_i/dt$) is comparable to the growth time of the instability.

Before onset of the high-frequency electron wave, the increase of electron temperature is small, since electron energy confinement time (≃ electron transit-time between end plates) is shorter than or comparable to the electron heating time. However, concomitant with the destabilization of the high-frequency wave, we observe a sudden electron temperature increase (Fig. 3), indicating strong wave heating.

3. Radial Gradients of T_e and u :

At low currents, Fig. 21, drift velocity shear and stronger electron heating at the plasma edge are observed, as expected from the initial radial density distribution (see Fig. 1). For $V_{appl} > 2.5$ V , the HF electron wave destabilizes in the region where drift velocity and drift velocity shear are high. With increased V_{appl} , the instability increases in intensity and spreads to the center of the plasma; simultaneously, drift velocity and electron temperature are equalized radially.

These results are explained qualitatively as follows. The parallel resistivity increases beyond onset of the continuous ICDW, which in turn reduces thermal electron-conduction loss to the end-plates. But the continuous ICDW does not produce enough perpendicular heat transfer to flatten the radial electron temperature profile, and thus does not affect the current profile. Once the high-frequency electron wave is generated, this instability induces anomalous interactions between electrons, invoking both anomalous electron viscosity and perpendicular conductivity. Observations of onset frequency, long wavelength, a bump-on-tail (runaway) electron distribution are in agreement with the

properties of Gould-Trivelpiece modes. Moreover, this type of high-frequency instability has been predicted to produce anomalous electron viscosity by electrostatic turbulence.[39,40]

4. Sheath Effects:

Plasma behavior in linear devices may be dominated by effects due to the presence of endplate sheaths. Special consideration must therefore be given to a detailed relation between observed plasma effects and their cause, i.e, either sheath or bulk plasma phenomena.

Endplate sheath effects have been shown to affect Q-device equilibrium,[41,42] transport phenomena,[42,43] I-V-characteristics,[5,6] and plasma temperature.[44] In the present experiment we confirm in detail that the instabilities and their resultant effects are not due to sheath phenomena but are effects of the bulk plasma.

(a) In the stable regime we observe classical resistivity in agreement with the Spitzer value, confirming Rynn's earlier and more detailed measurements on the negligible contribution of sheath resistivity at the higher densities.[6]

(b) In the stable and unstable regimes resistivity measured externally from the I-V characteristic agrees well with internally, locally measured values from an rf conductivity probe, again indicating that sheath resistivity can be neglected.

(c) The detailed identification of the instabilities observed relates these instabilities to sources of

free energy of the bulk plasma not connected to the sheaths, and the instability is observed to grow in the bulk plasma, away from the sheaths. Electron acceleration through the sheaths is not present for the electron-rich conditions of the experiment.

(d) The effect of ion heating by sheath acceleration in the presence of the instability was negligible: pulsed experiments show that the ion heating time is much shorter than the ion transit-time, but comparable to a few instability growth times. Radial sheath acceleration should scale with 1/B, which was not observed.

(e) The increased resistivity observed after instability onset scales with instability amplitude as expected and occurs during times faster than the ion transit-time, but comparable to a few instability growth times, indicating that the anomalous resistivity is instability-caused.

(f) The density decrease was not considered in detail but appears to be clearly generated by the current-driven drift instability, as described elsewhere.

D. Theoretical Explanation for Anomalous Transport Phenomena

In unstable plasmas, fluctuations are greatly enhanced over the thermal equilibrium level, and scattering of individual particles by collective fluctuation fields due to instabilities becomes a principal dissipation mechanism.

In the present experiment, the electron current induced by an externally applied electric field parallel to B together with radial plasma inhomogeneities drives the plasma into a turbulent state by exciting various microinstabilities. In this process momentum and energy of the parallel electron drift are fed into the waves and then dissipated into thermal energy of particles. Diffusion coefficient, resistivity, thermal conductivity, viscosity, and as a result, heating rates of plasma particles are strongly affected by the turbulent fluctuations.

The wave-induced anomalous resistivity and the heating rate $d(nT_i)/dt$ of the ions are derived from the first moment of the electron Vlasov equation and the second moment of the ion Vlasov equation, respectively,

$$\eta = - \frac{1}{4\pi n_{eo}^2 e^2 u} \sum_{\vec{k}} \int d\omega k_z \mathrm{Im}\chi_e(\vec{k},\omega) < |E^2|(\vec{k},\omega) > \qquad (31)$$

and

$$\frac{d(n_i T_i)}{dt} = \frac{1}{6\pi} \sum_{\vec{k}} \int d\omega (\omega - \omega_i^*) \mathrm{Im}\chi_i(\vec{k},\omega) < |E^2|(\vec{k},\omega) > \quad , \qquad (32)$$

where $< |E^2|(\vec{k},\omega) >$ is the spectral function of the electric field fluctuations.[45] Equation (31) describes the parallel momentum transfer from electrons to waves. Similar results can be obtained

by a quasi-linear consideration.[46] Equation (32) shows energy transfer from the wave to ions. $\chi_e(\vec{k},\omega)$ and $\chi_i(k,\omega)$ represent polarizabilities of electrons and ions, as defined in Section II. $<|E^2|(k,\omega)>$ is related to the mean square value of the electron density fluctuations, which can be measured in the experiment with the aid of Poisson's and Parseval's theorems as

$$\tilde{\delta n_e^2} = \sum_{\vec{k}} \int d\omega <|n_e^2|(\vec{k},\omega)> = \sum_{\vec{k}} \int d\omega \left[\frac{k}{4\pi e} \mathrm{Re}\chi_e(\vec{k},\omega)\right]^2 <|E^2|(\vec{k},\omega)> \quad . \tag{33}$$

The angular brackets imply an average with respect to the spectral distribution $<|n^2|(k,\omega)>$ of the density fluctuations. Such an average can be evaluated by substituting values of the physical parameters measured at the peak of the wave spectrum.

As discussed in Section II, the explicit linear expressions for $\chi_e(\vec{k},\omega)$ and $\chi_i(\vec{k},\omega)$ depend on the parameters $(\omega-k_z u)/k_z v_e$, $(\omega-\omega_{ci})/k_z v_i$, and $\omega/k_z v_i$.

1. Discrete ICDW:

For the discrete, current driven ICDW, where $\omega - k_z u < k_z v_e$, $\nu_e < k_z v_e$ and $\omega_e^* < \omega$, we have $\mathrm{Re}\chi_e(\vec{k},\omega) = k_{De}^2/k^2$ and

$$\mathrm{Im}\chi_e(\vec{k},\omega) = \frac{k_{De}^2}{k^2}\left(\frac{\pi}{2}\right)^{1/2} \frac{\omega-k_z u-\omega_e^*(1-\mu_e/2)}{k_z v_e} \quad , \tag{34a}$$

$$\mathrm{Im}\chi_i(\vec{k},\omega) = \left(\frac{\pi}{2}\right)^{1/2} \frac{k_{Di}^2}{k^2} \sum_n \frac{\omega-\omega_i^*}{k_z v_i} I_n(b_i)$$

$$\times \exp\left[-b_i - \frac{(\omega-n\omega_{ci})^2}{2k_z^2 v_i^2}\right] \quad . \tag{34b}$$

Substituting Eqs. (34a) and (34b) into (31) and (32), we obtain the wave-induced resistivity and enhanced ion heating. From Eq. (34a), we conclude that a main anomalous-resistivity mechanism for the discrete-spectrum ICDW is wave-particle interaction through inverse Landau damping:

$$\eta_{anom} \simeq \frac{(2\pi)^{3/2}}{2\omega_{pe}} \frac{\langle k_z \rangle}{k_{De}} \left\langle \left(\frac{\tilde{n}_e}{n_{eo}}\right)^2 \right\rangle \quad . \tag{35}$$

Thus, for the experimental conditions, $\eta_{class}/\eta_{anom} \simeq 0.05$ to 0.3, for $\tilde{n}_e/n_{eo} \simeq 0.1$, which agrees well with the measurements shown in Table 1 and Figs. 2, 10; $(k_\perp \rho_i \simeq 1 \ , \ \omega/k_z \simeq u/2)$. Note that this result is only valid for the linearly growing stage of the instability; at the highly nonlinear stage a new description of χ_e should be invoked, or stochasticity has to be introduced in $\langle E^2(\vec{k},\omega)\rangle$.

The enhanced ion heating rate can be derived in a similar way $(\omega^* < \omega_{ci})$ as

$$\frac{1}{T_i}\frac{dT_{i\perp}}{dt} \simeq (2\pi)^{1/2}\left(\frac{T_e}{T_i}\right)^2 \frac{u}{v_e}\,\omega_{ci}\,\frac{\tilde{n}_e^2}{n_{eo}^2} \quad , \tag{36}$$

where we have utilized the relation[14]

$$\frac{\omega}{k_z v_e} \simeq \frac{\omega}{k_z v_i}\, I_1(b_i)\exp(-b_i)\exp\left[-\frac{(\omega-\omega_{ci})^2}{2k_z^2 v_i^2}\right] \quad .$$

For the experimental conditions, $T_{eo} \simeq T_{io}$, $(\tilde{n}_e/n_{eo}) \simeq 0.1$, $(u/v_e) \simeq 0.2$, the heating time is deduced to be 200 to 500 μsec, which suggests relatively mild ion-cyclotron resonance heating in agreement with Fig. 2.[17] A similar result has been obtained for electrostatic ion-cyclotron waves excited by a filamentary current with $\omega_{e,i}^* = 0$.[47]

2. High-Frequency Drift Waves (Continuous ICDW):

For nonresonant high-frequency drift waves with $\omega > k_z v_e$, one expects highly nonlinear effects on resistivity from the steady-state turbulent spectrum in Fig. 3. Since $\nu_{ei} \ll \nu_{eff} < \omega$ and $\omega\nu_{eff} > k_z^2 v_e^2$ (ν_{eff} includes the wave-induced collision frequency), one employs Eq. 26 with ν_{ei} substituted by ν_{eff} for dispersion relation. With $k_\perp^2\rho_i^2 \gg 1$,

$$\left.\begin{aligned} \mathrm{Re}\chi_e &= \frac{k_{De}^2}{k^2}\,\frac{\omega_e^*}{\omega} \quad , && (37a)\\ \mathrm{Im}\chi_e(\vec{k},\omega) &= 1.96\,\frac{k_{De}^2}{k^2}\,\frac{k_z^2 v_e^2}{\omega\nu_{eff}}\left[1-\frac{\omega_e^*}{\omega}(1+1.71\mu_e)\right] \quad , && (37b)\end{aligned}\right\}$$

and

$$\mathrm{Im}\chi_i(\vec{k},\omega) = \left(\frac{\pi}{2}\right)^{1/2} \frac{k_{Di}^2}{k^2} \frac{\omega-\omega_i^*}{kv_i} \exp\left(-\frac{\omega^2}{2k^2v_i^2}\right) . \qquad (37c)$$

Substituting (37a) and (37b) into Eq. (31), the anomalous resistivity induced by this instability is

$$\eta_{anom} \simeq 8\pi \frac{1}{\omega_{pe}} \frac{k_z}{k_{De}} \frac{\tilde{n}_e^2}{n_{eo}^2} \left(\frac{v_e}{u} \cdot \frac{k_z^2 v_e^2}{\omega \nu_{eff}}\right) (1.71|\mu_e|-2) \quad , (38)$$

with $\mu_e < 0, |\mu_e| > 1.2$; (Section II-C-4).

Furthermore, since

$$\eta_{total} = \eta_{class} + \eta_{anom} = \frac{m_e(\nu_{ei} + \nu_{anom})}{n_{eo}e^2} \equiv \frac{m_e \nu_{eff}}{n_{eo}e^2} \quad ,$$

$$\frac{\eta_{total}}{\eta_{class}} = \frac{1}{2}\left\{1+\left[1+8\left(\frac{k_z}{k_{De}}\right)\left(\frac{\omega_{pe}}{\nu_{ei}}\right)\left(\frac{\tilde{n}_e^2}{n_{eo}^2}\right)\left(\frac{v_e}{u}\frac{k_z^2 v_e^2}{\omega \nu_{ei}}\right)(1.71|\mu_e|-2)\right]^{1/2}\right\} \quad , \qquad (39)$$

where η_{class} denotes Spitzer-Härm (classical) resistivity.

We note that the mechanism generating anomalous resistivity for the continuous, nonresonant ICDW is different from that for the current-driven discrete ICDW or of ion sound, i.e., from inverse Landau damping, where $u > \omega/k_z$. The continuous ICDW is nonresonant, $u << \omega/k_z$, and thus not driven mainly by the parallel electron current but by the radial pressure inhomogeneity. A strong T_e-gradient develops due to electron heating by the current near the edge of the plasma column. When the ΔT_e-determined diamagnetic electron drift velocity,

$(1/n_e)(dn_e/dx)T_e/m\omega_{ci}(1.71|\mu_e| - 1)$, exceeds the perpendicular phase velocity, $\omega/k_y \simeq v_i^*$, electron momentum is transferred to the wave. Thus, anomalous resistivity can occur in an inhomogeneous plasma even when $u<\omega/k_z$, if a plasma inhomogeneity drives the instability.

Substituting values of experimental parameters, $k_z(0.02 \rightarrow 0.1)$, $k_y(10 \rightarrow 60\ cm^{-1})$, $v_e(0.3 \rightarrow 1\times10^8 cm/sec.)$, ν_{ei} $(0.5 - 10\times10^6 sec^{-1})$, $\mu_e(-5 \rightarrow -2)$, $\tilde{n}_e^2/n_{eo}^2 \simeq 10^{-2}$ to 10^{-3} , the calculated anomalous resistivity is rather small $(\eta_{anom}/\eta_{class} \lesssim 1)$ compared with the observed value $(\eta_{exp}/\eta_{class} \gtrsim 10)$ in the steady-state experiment. Although this discrepancy is not fully explained at the moment, it suggests the presence of highly nonlinear mechanisms. Note that Eq. (31) gives parallel resistivity for comparison with the I-V plots. The anomaly in the perpendicular resistivity is expected to be stronger, but was not measured explicitly.

Finally, we calculate the turbulent ion heating rate resulting from this instability. For a monochromatic wave, one would obtain the ion heating rate by substituting Eq. (37c) into Eqs. (32) and (33):

$$\frac{1}{T_i}\frac{dT_{i\perp}}{dt} = \left(\frac{\pi}{2}\right)^{1/2} \left\langle \frac{(\omega-\omega_i^*)^2}{\omega} \frac{\omega}{kv_i} \exp\left(-\frac{\omega^2}{2k^2v_i^2}\right)\right\rangle \frac{\tilde{n}_e^2}{n_{eo}^2} , \tag{40}$$

which would give a rather slow heating rate $\omega=(\omega_i^*/1+k^2\lambda_{Di}^2)$. To consider the stochasticity of the fluctuation field, we introduce a correlation time $1/\nu(\vec{k})$ for a fixed value of $\vec{k}$,[48]

$$\langle |E^2(\vec{k},\omega)| \rangle = |E_k|^2 \frac{\nu(\vec{k})/\pi}{[\omega-\omega(\vec{k})]^2+\nu(\vec{k})^2} \tag{41}$$

where

$$\omega(k) = \frac{\omega_i^*}{1+k^2\lambda_{di}^2} .$$

Then, for $\nu(\vec{k}) << \omega(\vec{k}) < kv_i$,

$$\frac{dT_{i\perp}}{dt} \simeq \omega_{pi}^2 \sum_{\vec{k}} \frac{\langle |E_k^2| \rangle}{4\pi n_{io}} \left[\frac{\nu(\vec{k})}{k^2v_i^2} + \left(\frac{\pi}{2}\right)^{1/2} \frac{(\omega-\omega_i^*)^2}{k^3v_i^3} \exp\left(-\frac{\omega^2}{2k^2v_i^2}\right)\right] . \tag{42}$$

The first term in the right side represents nonresonant (stochastic) heating. For experimental conditions, the second (resonant heating) term is rather small $(\omega \simeq \omega_i^*)$.

Substituting measured values of $\sum_k \langle E_k^2 \rangle / 4\pi n_o T_{io} \simeq 0.005 \rightarrow 0.01$, $ku_i = \frac{1}{2}\omega_{peak}$, $\omega_{peak} \simeq \frac{1}{3}\omega_{pi} \simeq 1$ MHz $\times (2\pi)$, and $[\nu(\vec{k})/\omega_{peak}] = 0.02 \rightarrow 0.05$ [$\nu(k)$ was roughly measured by taking cross-correlations between the two signals from the

probes separated by $\lambda_y = 2\pi/k_{peak}$] , one obtains $\tau_{heating} \simeq 3$ to 12 μsec , which agrees with the observations in Fig. 11. Thus, the ion heating observed agrees with the estimate based on stochastic heating by high-frequency drift waves.

V. DISCUSSION AND CONCLUSION

The present experiments were performed in a plasma where the equilibrium is well understood, the free-energy reservoirs available for driving instabilities are limited in number and known, and impurities and neutrals are negligible. In contrast to other current-driven instability work, the ratio of electron-to-ion temperature is close to one, and density and temperature inhomogeneities are significant. Thus, ion sound is ion Landau damped and diamagnetic-drift waves (which are propagating in the perpendicular direction and are therefore not ion Landau damped) play a dominant role and generate anomalous effects normally connected with ion sound in homogeneous, $T_e/T_i \gg 1$, plasmas. The low-temperature-ratio regime, $T_e/T_i \lesssim 1$, is relevant and probably necessary for fusion reactors.

Dispersion relations for the different instabilities are derived from general dielectric constants, and consider specific phase velocity and frequency regimes. The slab model includes radial density and temperature gradients, thermal and electric conductivity, ion viscosity, and effects of parallel electron current. For $|\omega_i^*| < \omega_{ci}$, high-frequency instabilities with $\omega_{i,e}^* < \omega_{ci}$ can only be excited by resonant interaction between parallel electron current and wave; for $|\omega_{i,e}^*| > n\omega_{ci}$, drift waves with discrete- or continuous-frequency spectra up to $n\omega_{ci}$ $(n \lesssim 10)$ can be destabilized due to the plasma inhomogeneity; the negative temperature gradient $(\nabla_r T/\nabla_r n < -1)$ produced by parallel electron current in the experiment increases instability growth rates.

Four instabilities destabilizing consecutively with increased electron-drift velocity (current) were identified by measurements of ω and k. Three of these are modes of the inhomogeneous plasma propagating azimuthally with the diamagnetic-drift velocity. The ion-cyclotron drift wave with continuous spectrum (the third instability destabilized) has special significance: Frequency spectrum and anomalous effects produced are similar to those expected from ion sound, and these drift waves can be destabilized in plasmas which are ion-sound stable. This continuous-spectrum ICDW is driven by the negative temperature gradiant and propagates azimuthally with $(\omega/k_y) \simeq v_{di}^*$.

It is the high-frequency drift wave (continuous ICDW) which generates anomalous resistivity, current inhibition, and strong radial losses in the isothermal, inhomogeneous plasma, when ion sound is ion Landau damped, i.e., $T_e \simeq T_i$. Anomalous resistivity measurements were monitored by a rf conductivity probe to eliminate the sheath effects on I-V characteristics through the plasma ends, and it was shown that the observed enhanced resistivity is due to wave-particle interaction in the bulk plasma. Intense ion heating was detected concomitant with the onset of the ion-cyclotron drift waves with discrete $(T_i/T_{i0} \simeq 3)$ and continuous $(T_i/T_{i0} \simeq 10)$ spectra. This turbulent ion heating was investigated further in pulsed operations, and it was found that the ion heating time is comparable to several instability growth times.

A detailed comparison between the calculated and the observed anomalous resistivity and turbulent

ion heating by the ion-cyclotron drift waves with both discrete and continuous spectra shows that while the intense ion heating can be theoretically explained by taking into account the stochasticity of the wave, there remains a discrepancy between the theoretical and experimental anomalous (parallel) resistivity.

ACKNOWLEDGMENT

This work was supported by the United States Energy Research and Development Administration, Contract No. E(11-1)-3073.

REFERENCES

1 S. M. Hamberger, J. Jancarik, Phys. Fluids 15, 825 (1972).

2 S. Q. Mah, H. M. Skarsgard, A. R. Strilchuk, Phys. Rev. Lett. 25, 1409 (1970).

3 A. Hirose, I. Alexeff, W. D. Jones, S. T. Kush, K. E. Lonngren, Phys. Rev. Lett. 25, 1563 (1970).

4 R. W. Motley, "Q Machines," Academic Press (1975).

5 N. Rynn, Phys. Fluids 5, 635 (1962).

6 N. Rynn, Phys. Fluids 7, 284 (1964).

7 E. Hinnov, J. Hirshberg, F. Hofman and N. Rynn, Phys. Fluids 7, 284-291 (1975).

8 S. Watanabe and H. Tanaka, J. Phys. Soc. Jpn.36, 1661 (1974).

9 N. S. Buchelnikova, R. A. Salimov and Yu. I. Eidelman, Zh. Tekh. Fiz. 37, 1477-1967 (1967); Sov. Phys.--Techn. Phys. 12, 1073 (1968).

10 N. S. Buchelnikova and R. A. Salimov, Zh. Eksp. Teor. Fiz 60, 1108-1119 (1969); Sov. Phys. JETP 29, 595 (1969).

11 R. Ellis and R. W. Motley, Phys. Fluid 17, 582 (1974).

12 T. C. Simonen, T. K. Chu and H. W. Hendel, Bull. Am. Phys. Soc. 15, 532 (1970).

H. W. Hendel and M. Yamada, Bull. Am. Phys. Soc. 18, 1312 (1973); Proceedings AISNE Conf., Sidney, 26-1 (1975).

13 E. A. Jackson, Phys. Fluids 3, 786 (1960).

14 W. E. Drummond and M. N. Rosenbluth, Phys. Fluids 5, 1507 (1962).

15 B. Coppi, E. Mazzucato, Phys. Fluids 14, 134 (1971).

16 H. W. Hendel, M. Yamada, Phys. Rev. Lett. 33, 1076 (1974).

17 M. Yamada, H. W. Hendel, S. Seiler and S. Ichimaru, Phys. Rev. Lett. 34, 650 (1975).

18 A. A. Rukhadze and V. P. Silin, Usp. Fiz. Nauk. 96, 87 (1968); Sov. Phys. VSPEKHI 11, 659 (1969).

19 S. Ichimaru, "Basic Principle of Plasma Physics," Chapter 8, W. A. Benjamin, Inc., New York (1974).

20 P. L. Bhatnagar, E. P. Gross, and M. Krook, Phys. Rev. Lett. 94, 511 (1954).

21 L. S. Bodgenkvich and A. A. Rukhadze, Zh. Eksp. Teor. Fiz. 51, 628 (1966); Sov. Phys. JETP 24, 418 (1967).

22 A. B. Mikhailovskii and A. V. Timofeev, Zh. Eksp. Teor. Fiz. 44, 919 (1963); Sov. Phys. JETP 17, 626 (1963).

23 A. B. Mikhailovskii, Theory of Plasma Instabilities, Vol. 2, Consultants Bureau, New York (1974).

24 M. Yamada, S. Seiler, H. W. Hendel and H. Ikezi, Phys. Fluids 20, 450 (1977).

25 D. K. Bhadra, Plasma Physics 15, 1185 (1973).

[26] M. K. Hudson, Phys. Fluids 18, 1077 (1975).

[27] J.P.M. Schmidt, J. Plasma Phys. 12, 51 (1974).

[28] B. D. Fried and S. D. Conte, "The Plasma Dispersion Function," Academic Press, New York (1961).

[29] I. Katsumata and M. Okazaki, Jpn. J. Appl. Phys. 6, 123 (1969);
R. W. Motley and T. Kawabe, Phys. Fluids 14, 1019 (1971).

[30] R. A. Olson and E. C. Lary, Rev. Sci. Instr. 33, 1350 (1962); AIAAJ.1, 2513 (1963).

[31] P. Korn and C. B. Wharton, J. Appl. Phys. 42, 4828 (1971).

[32] H. W. Hendel and T. K. Chu, Methods of Experimental Physics (Academic Press, New York, 1970), Vol. 9A, Chapter 9.
J. Walsh, S. P. Schlesinger, K. Josephy and T. C. Marshall, Phys. Fluids 12, 2374 (1969).

[33] N. Rynn, D. R. Dakin, D. L. Louvell, and G. Benford, Phys. Rev. Lett. 33, 765 (1974).

[34] H. W. Hendel, T. K. Chu and P. A. Politzer, Phys. Fluids 11, 2426 (1968).

[35] P. A. Politzer, Phys. Fluids 14, 2410 (1971).

[36] N. D'Angelo and R. W. Motley, Phys. Fluids 5, 633 (1962).
R. W. Motley and N. D'Angelo, Phys. Fluids 6, 296 (1963).

[37] A. W. Trivelpiece and R. W. Gould, J. Appl. Phys. 30, 1784 (1959).

[38] A. Bers, B. Coppi, T. Dupree, R. Kulsrud and F. Santini, Proceedings of the Fourth International Conference on Plasma Physics and Controlled Nuclear Fusion Research, Madison, Wisconsin, 1971 (International Atomic Energy Agency, Vienna, 1972), paper CN-28-E16.

[39] A Hirose, S. Q. Mah, H. M. Skarsgard, A. R. Strilchuk and D.W.A. Whitfield, Phys. Rev. Lett. 28, 1185 (1972). W. Horton, Jr., Phys. Rev. Lett. 28, 1506 (1972).

[40] A. Hirose and I. Alexeff, Phys. Fluids 16, 1087 (1973).

[41] S. v. Goeler, Phys. Fluids 7, 463 (1964).

[42] N. D'Angelo and N. Rynn, Phys. Fluids 4, 1303 (1961).

[43] N. Rynn, Phys. Fluids 9, 165 (1966).

[44] N. D'Angelo and A. Y. Wong, Phys. Fluids 8, 757 (1965).

[45] T. Tange and S. Ichimaru, J. Phys. Soc. Jpn. 36, 1437 (1974).

[46] R. Z. Sagdeev and A. A. Galeev, Nonlinear Plasma Theory, W. A. Benjamin, New York (1969).

[47] D. R. Dakin, T. Tajima, G. Benford and N. Rynn, J. Plasma Phys. 15, 175 (1976).

[48] S. Ichimaru, J. Phys. Soc. Jpn. 39, 1373 (1975).

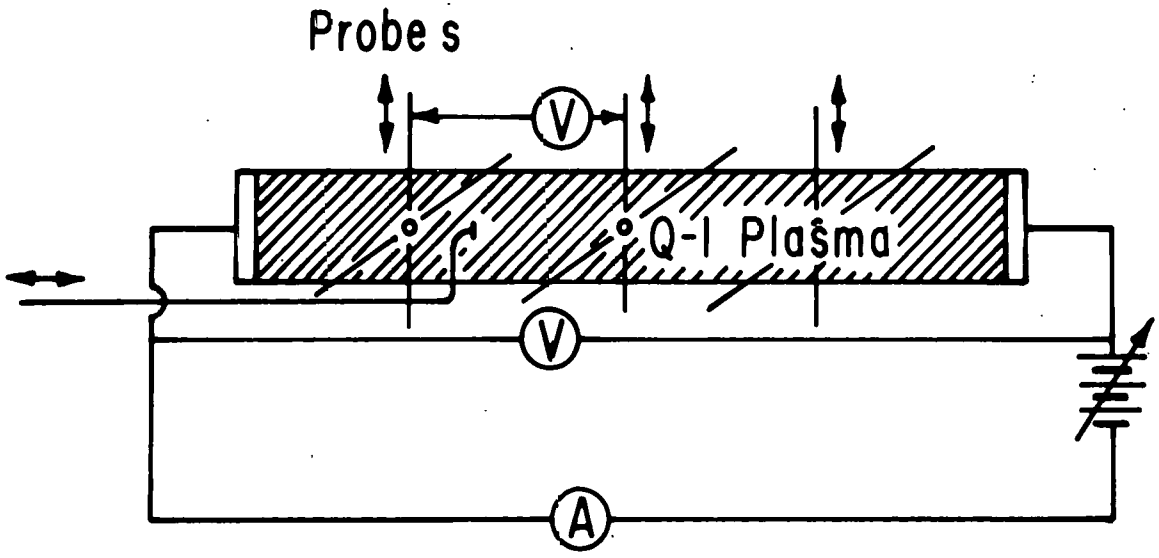

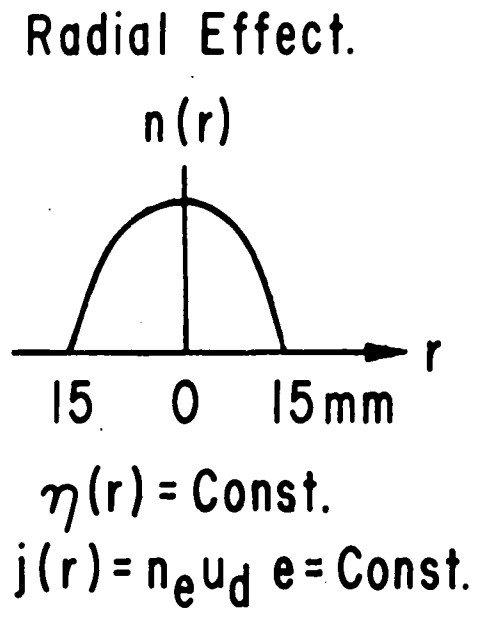

773174

Fig. 1. Diagram of experimental set-up.

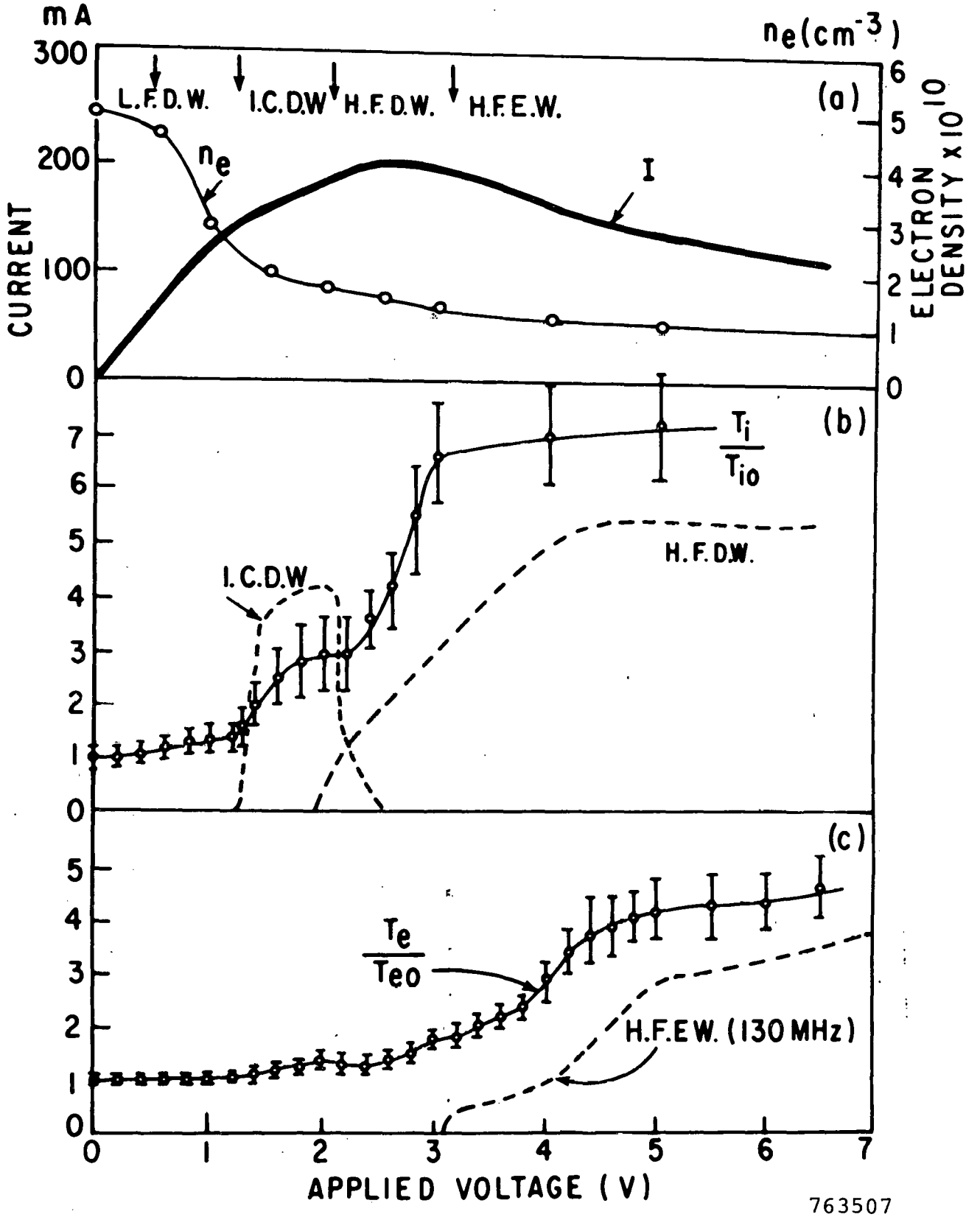

Fig. 2. Measured plasma parameters vs V_{appl}. (a) Current and density; arrows indicate instability onsets. B = 6 kG, T_{eo} = 0.3 eV, T_{io} = 0.4 eV. (b) Normalized ion temperature and amplitudes of ICDW and HFDW. (c) Normalized electron temperature and high-frequency electron instability amplitude.

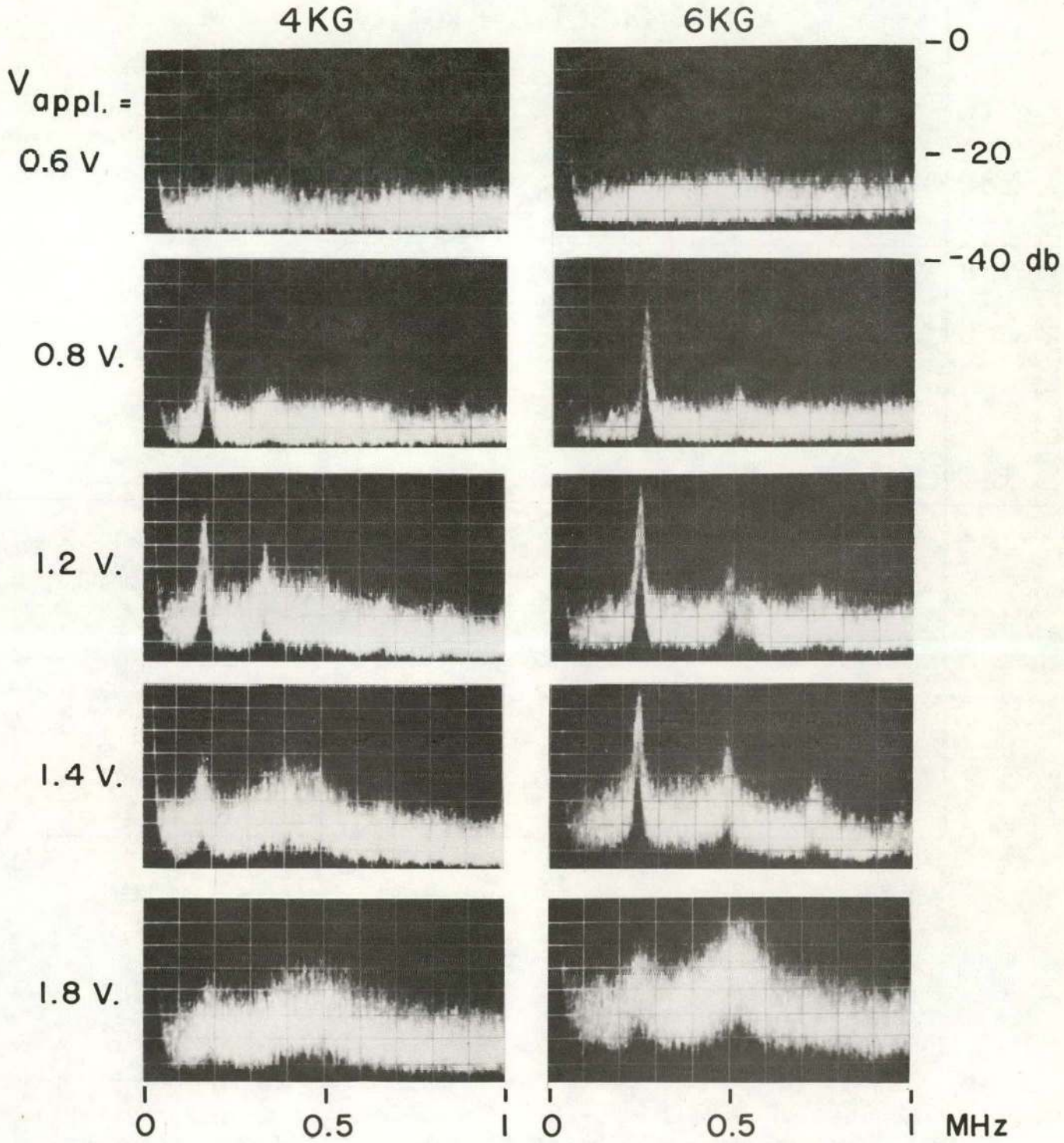

743373

Fig. 3. Evolution of ICDW spectrum vs applied voltage. $n_e = 0.6 \times 10^{10}$ cm^{-3}.

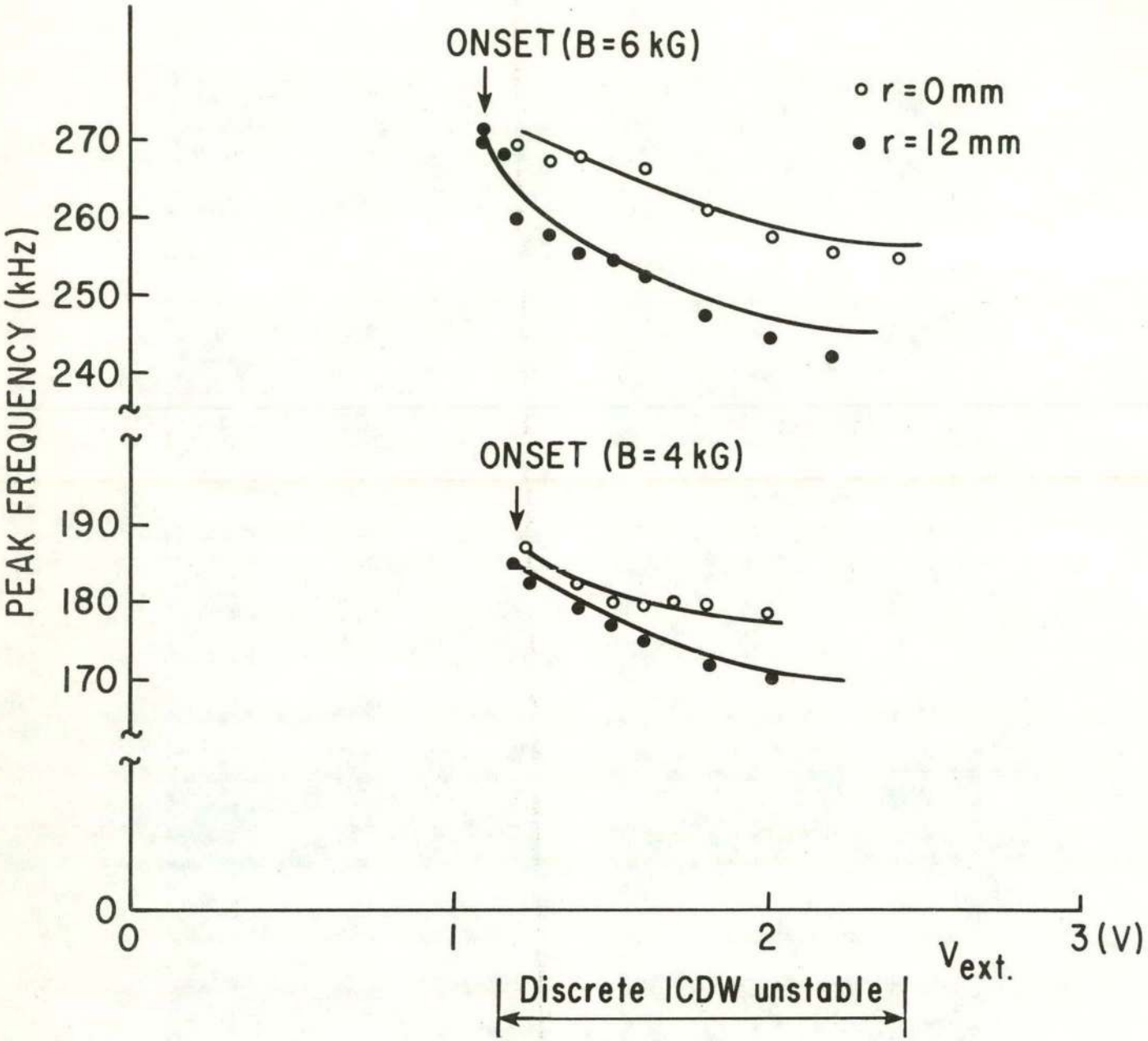

773172

Fig. 4. Peak frequencies of ICDW vs V_{ext} for two different B fields.

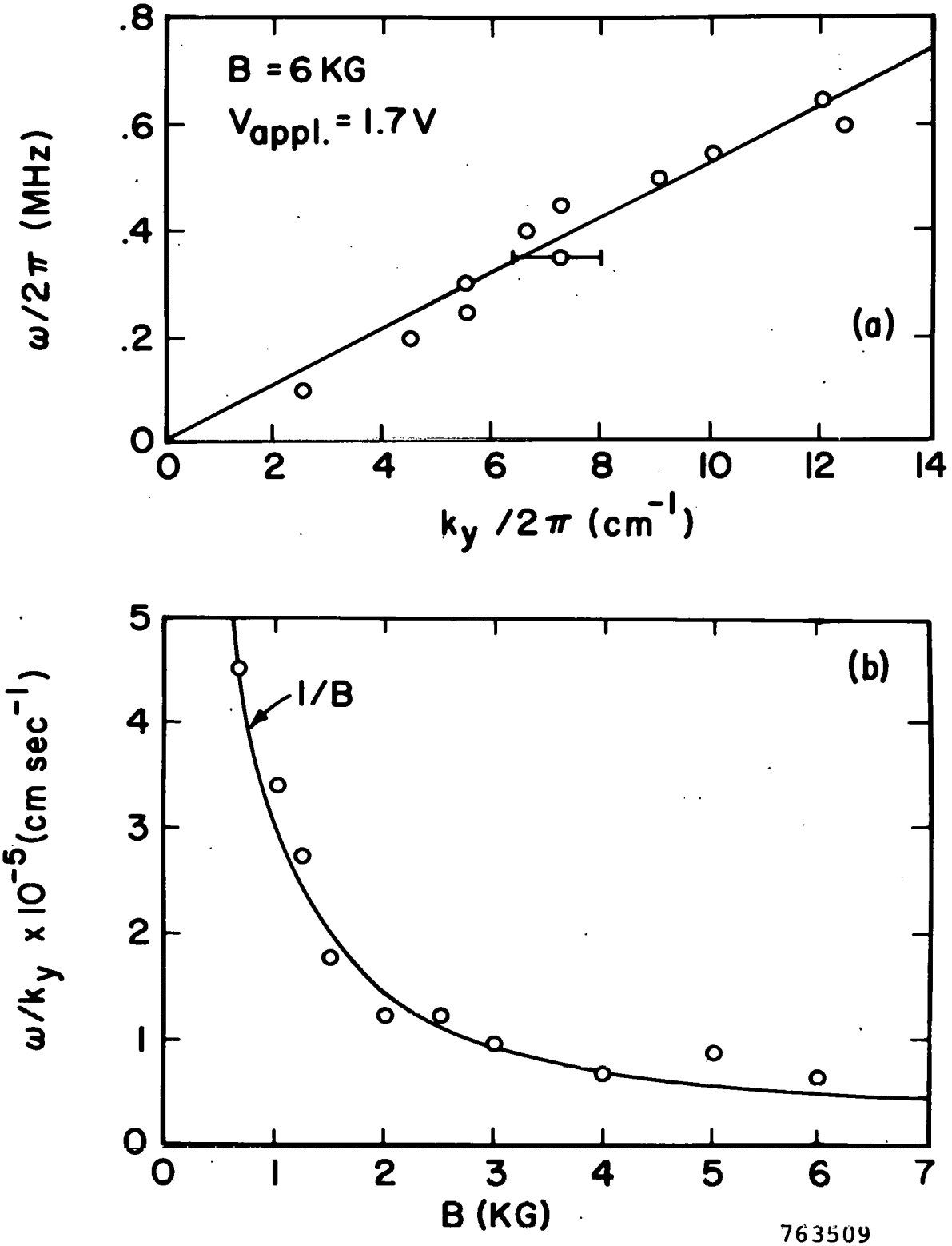

Fig. 5. Identification of HFDW (ICDW with continuous spectrum). (a) Measured dispersion relation; frequency vs azimuthal mode number. The solid line indicates $\omega = v_{di}^{*} k_y$. (b) Azimuthal phase velocity vs magnetic field strength. Solid curve shows $\omega/k_y = v_{di}^{*}(-V_{\underset{\sim}{E}\times\underset{\sim}{B}}) \propto 1/B$.

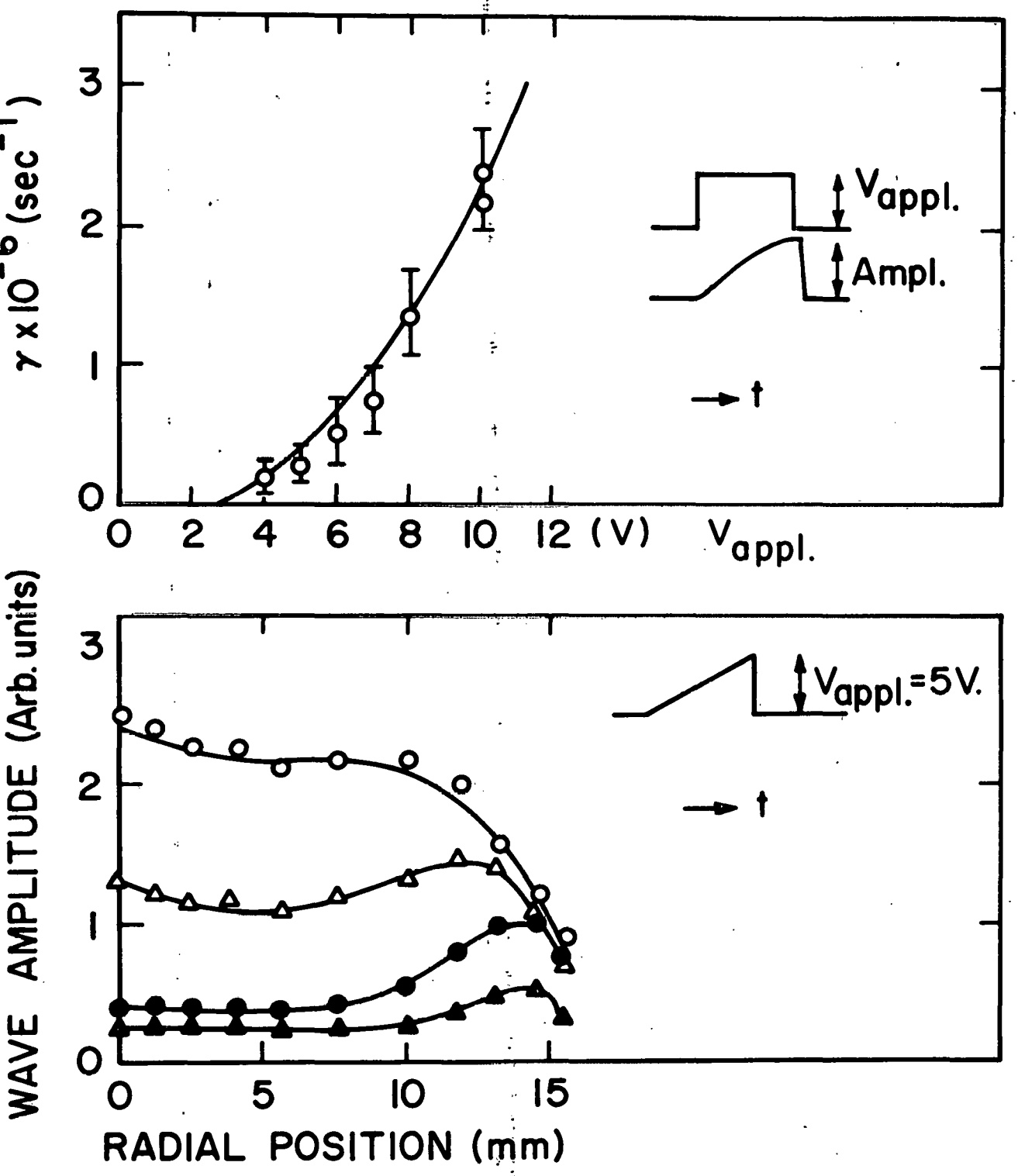

746124

Fig. 6. Temporal growth of HFDW, B = 4 KG, n = 1.5×10^{10}. (a) γ vs $V_{appl} \propto u$; pulse duration ≃ 50 μsec. (b) Evolution of radial profile of wave amplitude vs time; pulse duration ≃ 50 μsec. ▲t = 25 μsec; ● 30 μsec; Δ 35 μsec; o 40 μsec.

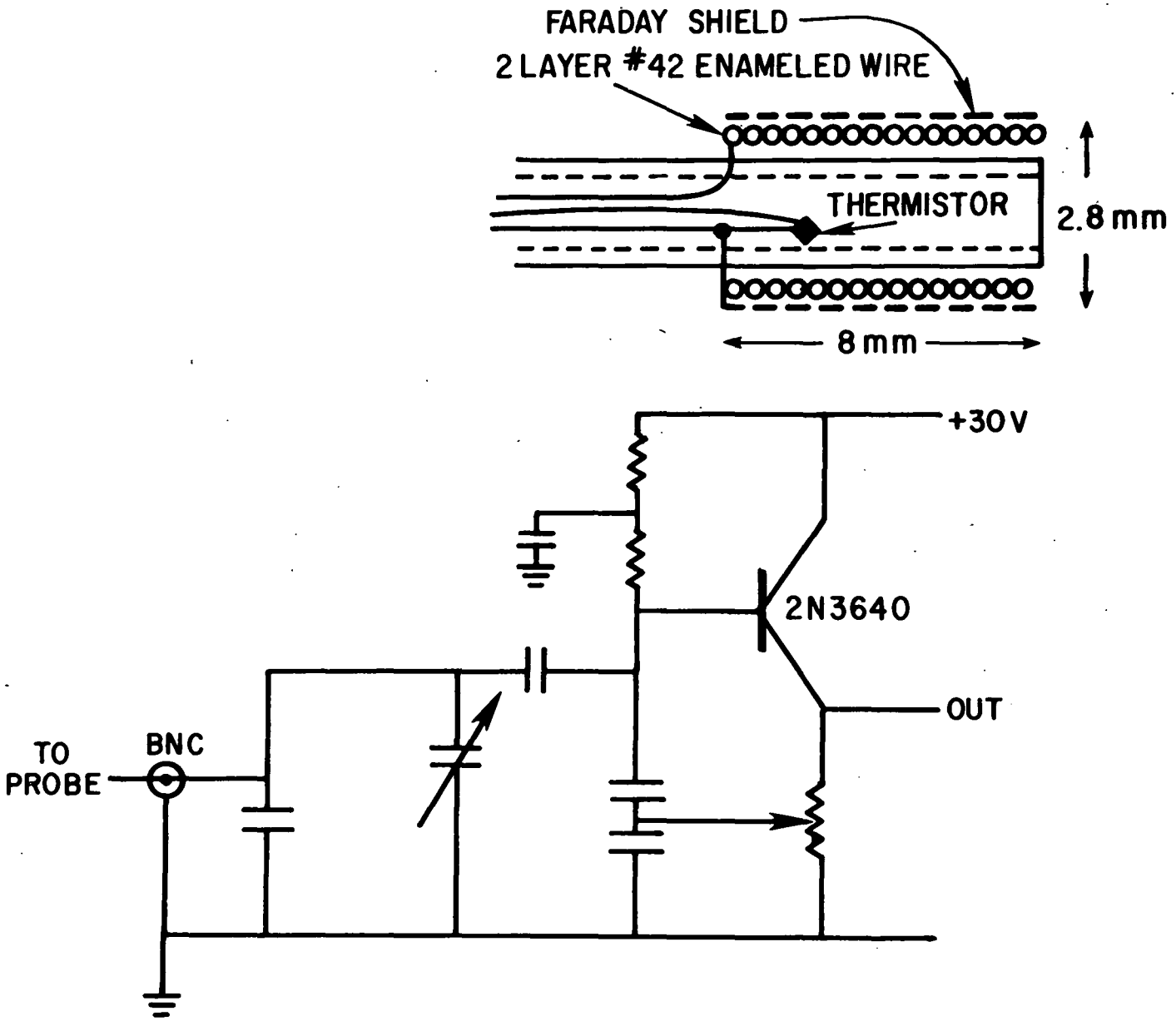

773173

Fig. 7. Diagram of rf conductivity probe and circuit.

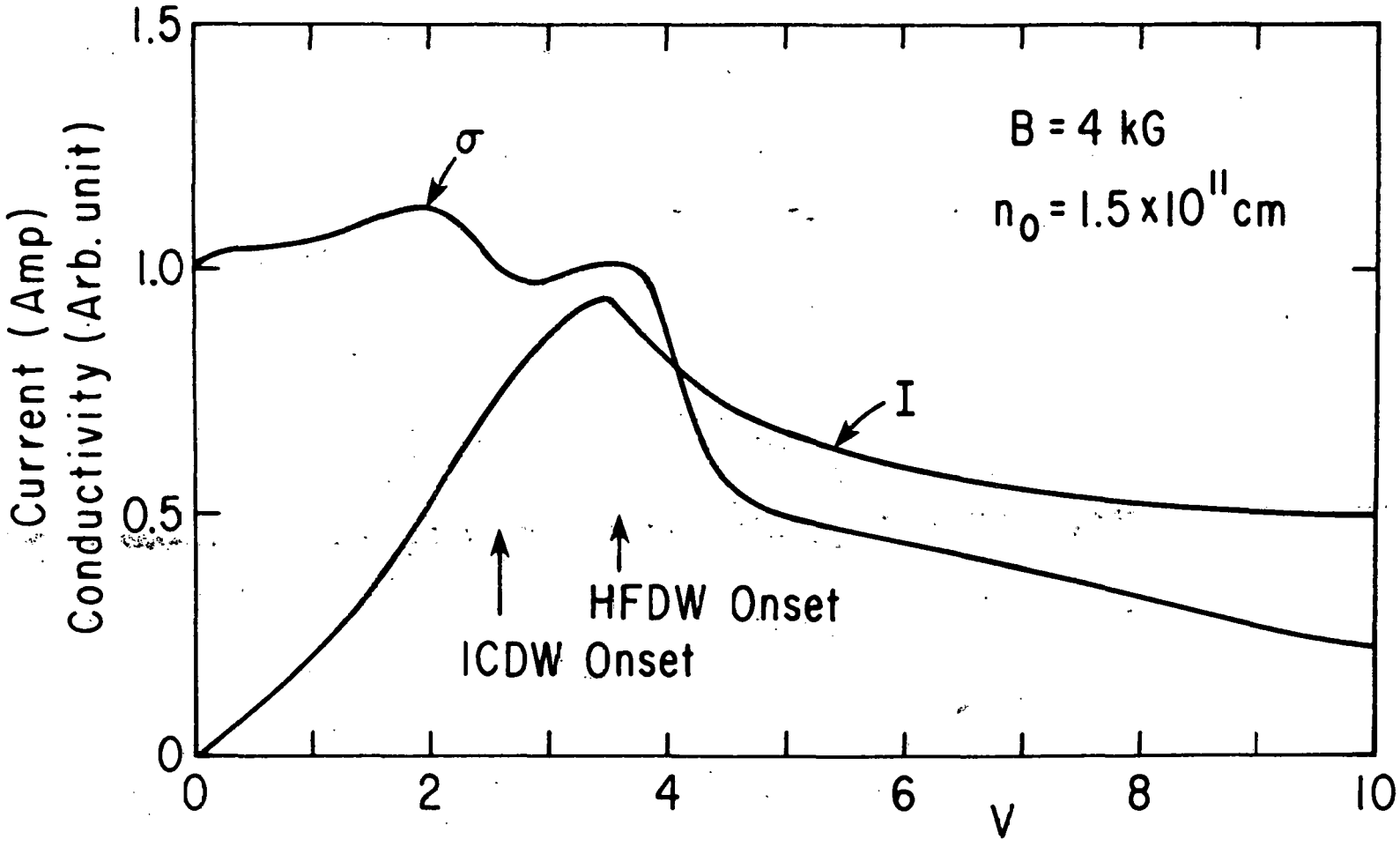

763146

Fig. 8. Measured internal conductivity and I-V curve.

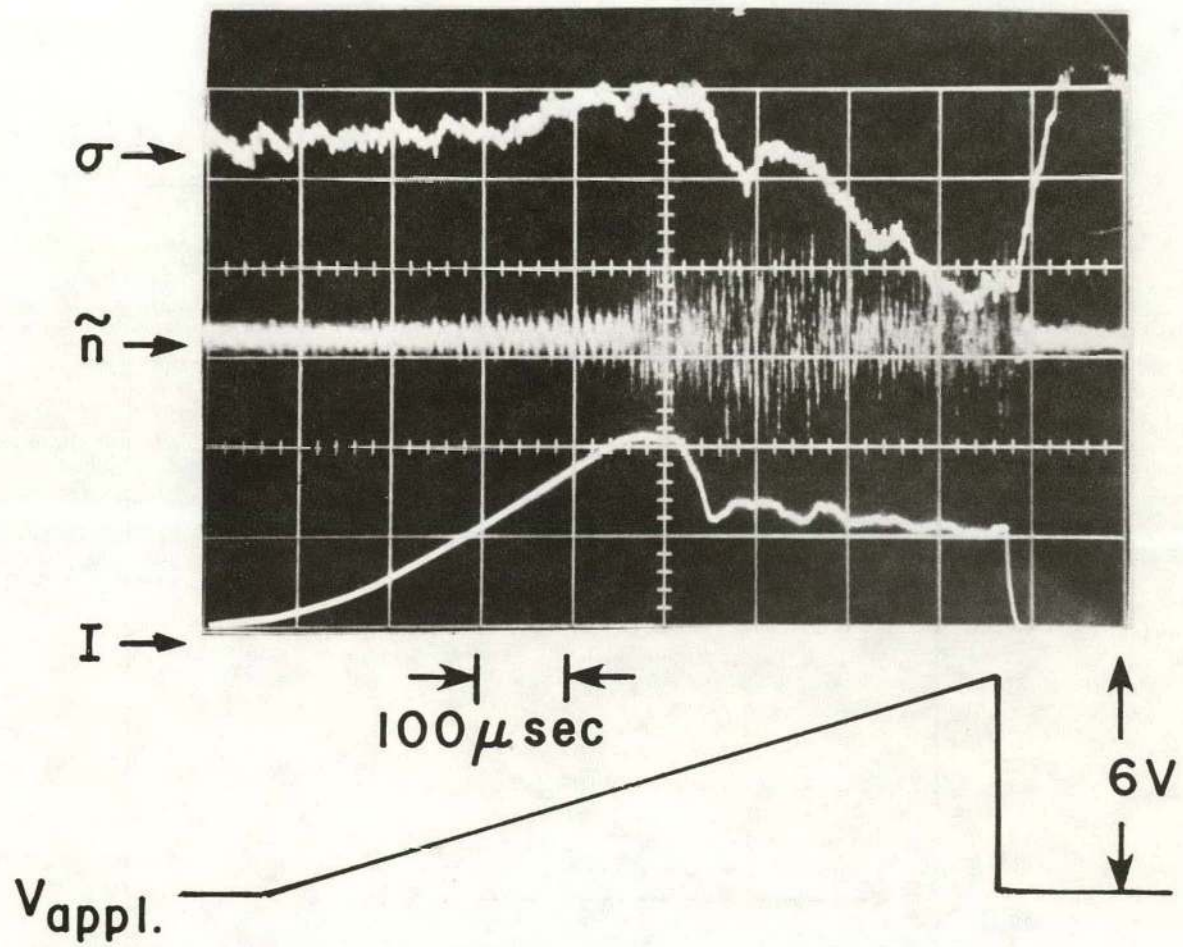

746125

Fig. 9. Time development of instability amplitude and conductivity.

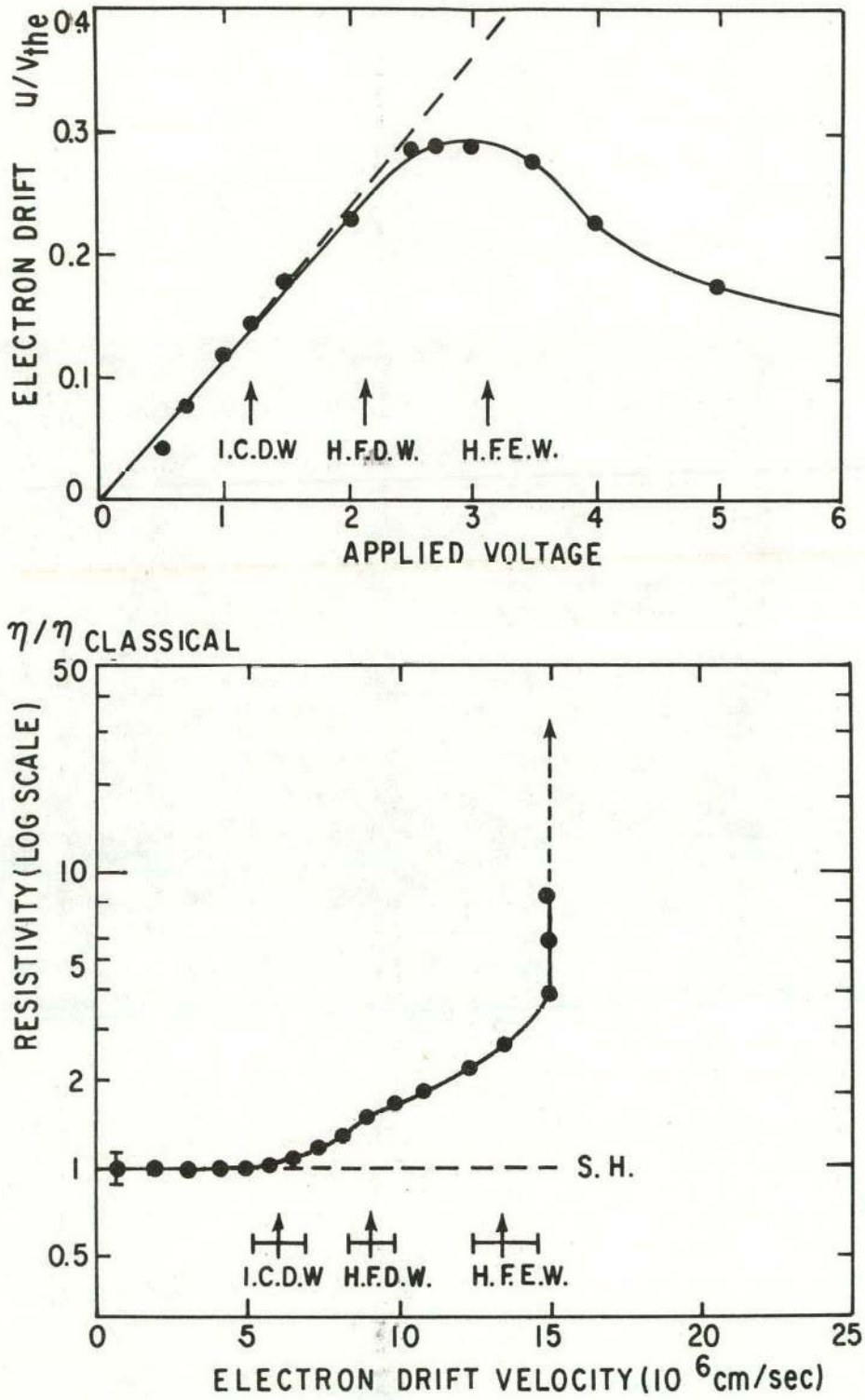

773171

Fig. 10. (a) Electron drift velocity vs V_{appl}. Decrease of u/v_{the} is due to increase of electron temperature. (b) Resistivity vs drift velocity. Plasma parameters as in Fig. 2. S.H. denotes Spitzer-Härm value.

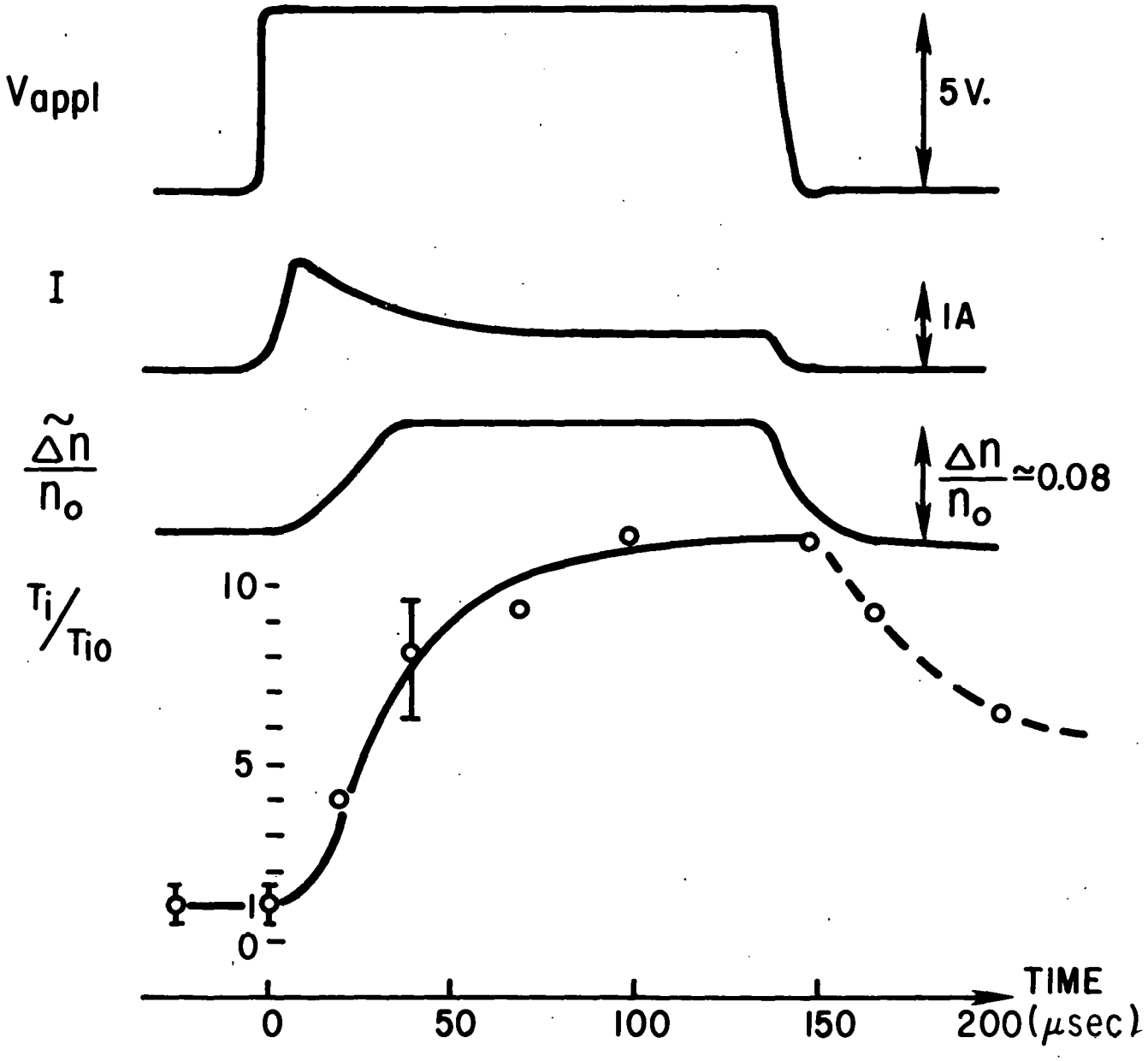

743906

Fig. 11. Time evolution of plasma parameters in pulsed operation. $n_e = 1.1 \times 10^{11}$ cm; B = 2 kG.

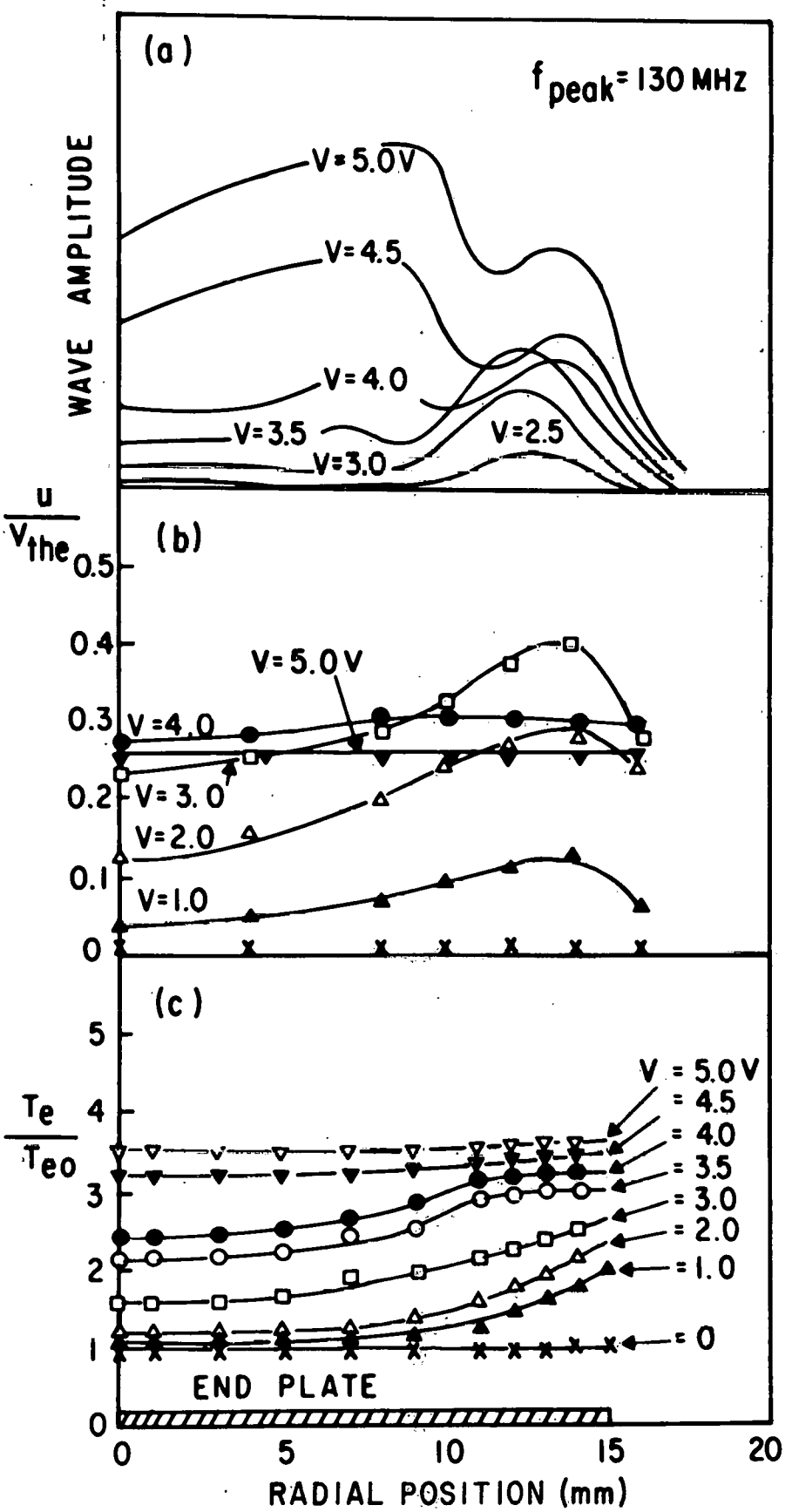

Fig. 12. Radial distribution of high-frequency electron wave amplitude (a), u/v_{the} (b), and T_e/T_{eo} (c), vs V_{appl}. Radial gradients (and peripheral current) relax with instability onset. Plasma parameters as in Fig. 2. $v_{the} = (8T_e/\pi m)^{1/2}$.

Instability	Threshold El. Current	Frequency Spectrum 10^3 10^4 10^5 10^6 10^7 10^8 (Hz)	Wavelength	Propagation	Anomalous Effects on Plasma
L. F. D. W.	$\frac{u}{v_{the}} = 0.03$	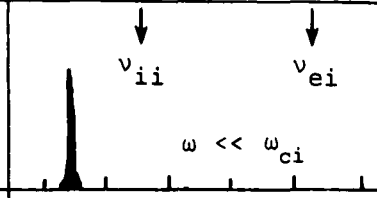	$k_y\rho_i<1$ $k_y>>k_z \sim \frac{\pi}{L}$	Azimuthal $\frac{\omega}{k_y} \approx v_e^*$	Anom. Diffusion
I. C. D. W.	$\frac{u}{v_{the}} \simeq 0.15$	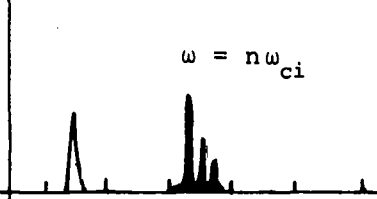	$(k_y\rho_i \sim 1)$ $\frac{\omega}{k_z} \simeq \frac{u}{2}$	Azimuthal	Ion Heating Anom. Resistivity (~30%)
H. F. D. W.	$\frac{u}{v_{the}} \simeq 0.20$	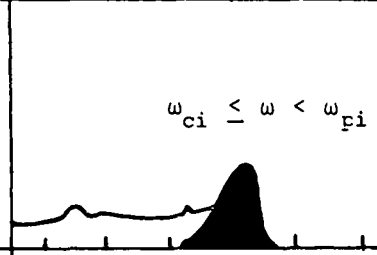	$k_y\rho_i>>1$ $\frac{\omega}{k_z} > v_{the}$	Azimuthal $\frac{\omega}{k_y} \simeq v_i^*$	Anom. Resistivity (10x) (Current Inhibition) Strong Ion Heating Electron Heating
H. F. El. W.	$\frac{u}{v_{the}} \simeq 0.3$	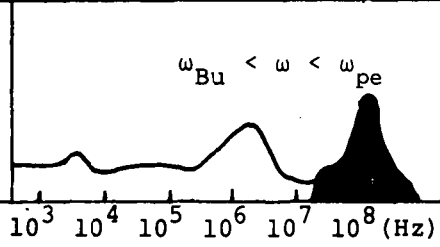			Strong Electron Heating Anom. Electron Viscosity $\left(\frac{du}{dr} \to 0 \quad \frac{dT_e}{dr} \to 0\right)$

773346

Table 1. Current-driven instabilities and resultant anomalies for Q-device plasmas. u denotes electron drift velocity, $v_{the} = (8T_e/\pi m)^{1/2}$.